University of Stavanger

Faculty of Science and Technology

MASTER'S THESIS

Study program/ Specialization: Petroleum Engineering - Drilling	Spring semester, 2013..... Open
Writer: Elyas Abdurehman Abubeker	…… (Writer's signature)
Faculty supervisor: Merete V. Madland External supervisor(s):	
Title of thesis: *Water Weakening of Chalks – Comparison of intact and fractured Cores*	
Credits (ECTS):30	
Key words: • Fractured and intact chalks • Water Weakening • Flooding brines • Rock mechanical tests • Hydrostatic tests • Creep	Pages: ……88…… + enclosure: ……N/A…… Stavanger, ……17.06.2013…….. Date/year

ABSTRACT

Even though Chemical induced compaction on high porosity chalks has been studied extensively, little attention was given to the impacts of fractures when chalk is exposed to various flooding brines. Due to the nature of fractures, the fluid transport mechanism down inside reservoirs is different between intact and fractured reservoirs and the observed results for intact high porosity chalk may not explain water weakening effects on fractured chalks. In addition, chemically induced weakening seems to be triggered by precipitation of secondary minerals which further cause increased dissolution. These new precipitates may be difficult to detect and quantify by conventional scanning electron microscope (SEM) investigations, however, from a previous experiment these precipitates could easily be found dominantly in the fracture.

The main objective of this study was to analyze and compare the effects of synthetic sea water (SSW), 0.219M $MgCl_2$ and 0.657M NaCl brines on the mechanical behavior of intact and fractured chalk samples, based on mechanical experiments carried out using hydraulically operated triaxial cells at 130^{o}C. Chemical analyses, porosity calculations and SEM analyses were made to further investigate fluid transport mechanisms and the formation of newly precipitated minerals.

The results showed that, independent of the type of brines, the presence of fractures inside the fractured cores resulted in lower chemical deformation compared to intact cores although the impact of fractures in reducing the deformation rate was magnified when the cores were flooded with SSW. However, the presence of fractures inside the tested cores had not totally stopped the water weakening effect as evidenced by the mechanical and chemical analyses results. This implied that the injected brines not only flow through the fractures but also diffused in to the core matrix to further cause deformation. This also fits very well with fracture/matrix model developed by Anderson & Evje (2012). Finally, SEM analysis results showed the formation of magnesium-bearing minerals at the fracture walls.

ACKNOWLEDGEMENT

I would like to express my most sincere appreciation to Dr. Reidar I. Korsnes for his infinite support and advice throughout the progress of this thesis. I will always admire his dedication and precision. I would also like to express my deepest gratitude to my supervisor Assoc. Professor Merete V. Madland for her excellent feedback and advice for the completion of this thesis.

Special appreciation goes to Kristine Geitle for her excellent collaboration during the experimental work. I would also like to thank Tania Hildebrand-Habel and Mona Minde for providing SEM images.

The greatest appreciation goes to my family who did everything for me from the moment I was born to the present. I would not be a person who I have become today without their help and positive attitude towards me. Furthermore, I would like to thank my friends for their comment and positive criticism.

Elyas Abdurehman Abubeker

TABLE OF CONTENTS

LIST OF FIGURES

LIST OF TABLES

1 INTRODUCTION

1.1 Background

The introduction of enhanced oil recovery techniques in the 20th century has helped the oil industry to be one of the economic giants of the world. Enhanced oil recovery techniques are implemented when there is a need to maximize the oil recovery after the natural drive mechanisms of the reservoir are depleted. This has been a success story in terms of extracting the maximum amount of oil and gas that could be recovered with today's technology. In North Sea, implementation of EOR techniques, such as sea water injection, has improved the oil recovery factor up to 50 percent (Sheng, 2011). However, little was understood about the impact of sea water injection on the mechanical behavior of the reservoir chalks when the injected water displaces the oil in place. It was not until the year 1984 subsidence of the overlying seafloor on Ekofisk reservoir, in the North Sea, was discovered and by January 1994 the subsidence had been reported to be reached 6 meters (Powell & Lovell, 1994). In line with the subsidence occurred in the Ekofisk field, water injection techniques was implemented to prevent the subsidence due to reservoir compaction as the pore pressure significantly reduced after oil production. Surprisingly, though, the water injection has not helped in reducing the reservoir compaction rate although the reservoir pressure was increased. This led to the conclusion that the water that is injected significantly weakens the reservoir rocks and gives extra room for additional reservoir compaction, and this phenomenon is known to be water weakening effect. This has received a great attention in the scientific community and opened new areas of research all over the world. At the University of Stavanger, great deals of experimental projects are going on subsidized by Norwegian government and petroleum companies.

In line with water weakening effects on chalk reservoirs, numerous experimental studies have been done on high porosity chalks to understand what is going on down in the reservoir pore spaces. Physical water weakening effects were taken as the main driving force and the chemical effects were neglected or assumed minor during

the early days. Most notably, the mechanism that was reported in many previous studies for water-chalk surface interactions is capillary effect (Delage, Cui, & Schroeder, 1996). It was argued that the capillary force that arises due to the presence of low saturations of water between the chalk grains acts as a glue to hold the grains together. During water injection, the water saturation inside the void spaces will increase and dissolve the water bridges that were initially binding the grains together. As a result, the capillary forces disappear and the chalk becomes weaker. However, Risnes & Flaageng (1999) experimental work on methanol saturated core samples showed water saturated core samples were much weaker than methanol saturated samples although methanol had the same effect as water in eliminating the capillary forces (since methanol is miscible with water). This showed capillary effect cannot be the only mechanism that explains water-chalk interactions but also chemical processes that might happen during water flooding. Moreover, Risnes et al. (2003) had performed several experimental tests with glycol and other types of brines as saturating fluids. Their results showed that both oil and glycol made the cores weaker compared to dry chalk and the cores were at their weakest point when flooded with water. This ultimately proved that water weakening effects were not only controlled by the physical parameters but also other parameters such as chemical processes.

Another interesting piece of work was shown when Korsnes et al. (2006) flooded chalk core samples with SSW and distilled water at high temperatures, such as 130^{o}C. Their results showed that, at 130^{o}C, chalks flooded with sea water were much weaker mechanically compared to chalks flooded with distilled water. This was not the case when the chalk samples were tested at ambient temperature. At ambient temperature, both sea water and distilled water flooded samples showed similar mechanical strength. Therefore, chemical reactions that were triggered at high temperatures had to be the reason for these variations in mechanical strength.

Korsnes et al. (2006) took the discussion ahead and hypothesized that substitution of Ca^{2+} with Mg^{2+} ions in the presence of sulfate and dissolution of chalk explains the water weakening effects during seawater injection. They argued replacement of Ca^{2+} with Mg^{2+} in the presence of sulfate would give extra room for compaction to occur as the Mg^{2+} ions are smaller in size than Ca^{2+}. However, M. Madland et al. (2008)

work on Kansas chalk samples flooded with seawater without the presence Mg^{2+} showed that considerable amount of compaction on the tested cores at 70 and 90^{o}C. Furthermore, recently, Madland et al. (2011) argued that the loss of magnesium in the core and the production of calcium cannot merely be the result of ion substitution process; rather their calculations showed that excessive loss of magnesium is explained by newly precipitated magnesium bearing minerals.

Having reviewed most of the papers on chemical induced compaction in chalk reservoirs, it is quite amazing to witness the deep understanding of the oil industry about the mechanisms behind water weakening effects. However, it seemed as though most of the works done previously had been focused on intact chalk core samples and little attention was given to the impacts of fractures inside chalk core samples. In addition, being the Ekofisk field reservoirs are naturally fractured, give us the motivation to further pursue and understand the impacts of fractures inside chalk core sample when flooding various brines. Therefore, the main objective of this study is analyze and compare the effects of flooding fluid content on the mechanical behavior of intact and artificially fractured Mons chalk core samples.

1.2 Problem Statement

Madland et al. (2011) verified over the hypothesis that precipitation of secondary minerals enhanced dissolution which can lead to increased creep. However, the experimental results presented from previous studies focus on high porosity intact chalks although the Ekofisk field reservoir is naturally fractured high porosity chalk. Due to the nature of fractures the fluid transport mechanism down inside reservoir is quite different between intact and fractured reservoirs and the observed results for intact high porosity chalk may not explain water weakening effects on fractured chalks. Therefore, further experimental work should be performed on fractured chalk core samples and a comparison should be made with intact chalk core samples.

1.3 Objectives

The best way, if not the only way, to predict the rock mechanical behaviors is to perform geomechanical studies using triaxial cells to simulate the real conditions in petroleum reservoirs. In North Sea, particularly in Ekofisk Field, the chalk reservoirs are becoming weaker and weaker resulting in considerable amount of sea bed subsidence. There is no doubt the in-situ stress state conditions would impact the mechanical nature of the rock but it would be a huge mistake if one assumed only physics is the reasons behind the weakening of the rocks. Because of the chemical nature of the injected fluids, chemistry as well plays an important role in weakening the chalk reservoirs. It is reasonable to assume the chalk reservoirs are under constant in-situ stress state conditions but they will still be continuously deforming because of time dependent effect known as creep. Creeping of the rocks in the reservoirs mainly magnified by the chemical injected during water injection. Chemically induced weakening seems to be triggered by precipitation of secondary minerals which further cause increased dissolution. These new precipitates may be difficult to detect and quantify by conventional SEM investigations, however, from a previous experiment these precipitates could easily be found dominantly in the fracture. Actually these precipitates seem to contribute to healing of these fractures (like kind of gluing the fracture together). Therefore, the objectives of this study are:

- To investigate the effects of injected fluid content on the mechanical behaviors of artificially fractured chalk samples and compare them with intact chalk core samples.
- To understand the governing mechanisms for water weakening effects on fractured as well as intact chalk reservoirs
- To estimate porosity reduction that may occur after mechanical test.
- To understand fracture/matrix flow. The results found here could be used to improve or validate fracture/matrix flow model developed by Anderson & Evje (2012).
- To detect or search for new minerals as the fracture core experiments make it easier to search for the minerals formed due to injection. The new minerals are expected to form dominantly in or nearby the fracture.

1.4 Scope of the Study

The scope of this study spans through four different experimental processes; 1) performing rock mechanical tests using hydraulically operated triaxial cells 2) Performing chemical analysis on water samples collected from the mechanical tests, 3) performing volume calculations to estimate post mechanical test chalk porosity reductions and 4) detecting minerals at the fracture wall by SEM-EDS analysis. The mechanical test procedures were designed in such a way that the effects of fluids content on the mechanical behavior of the chalk samples could be easily observed. For the first six days of the mechanical experiments, all core samples were flooded with 0.657 M NaCl brine. After six days, the flooding fluid was switched from NaCl to 0.219 M $MgCl_2$ brine or synthetic sea water (SSW) in order to observe the effects of $MgCl_2$ or SSW on creep strain, respectively. Three artificially fractured and two intact core samples were tested as shown in Table 1.1.

Table 1.1: Summary of the mechanical test procedure for all tested cores

Core Sample	Mechanical Test			Description
	Hydrostatic Phase	Creep Phase		
		The first six days	Remaining flooding period	
OB SV 12	Lasted for about 10 hours before the creep experiment started	NaCl	SSW	Fractured. 2mm hole was drill at center
OB SV 9		NaCl	SSW	Intact
OB SV 4		NaCl	$MgCl_2$	Fractured. 2mm hole was drill at center
OB SV 6		NaCl	$MgCl_2$	Intact
OB SV 18		NaCl	NaCl	Fractured. 2mm hole was drill at center

1.5 Outline of the Thesis

This thesis is comprised of seven chapters. Chapter 1 introduces the background study, problem statement, objectives and scope of study and important research topics. Chapter 2 delivers an update on literature reviews which have been done before. Chapter 3 presents the methodology of this thesis. Chapter 4 provides the detail results found from the mechanical tests, chemical analyses and porosity calculations. Chapter 5 discusses the main findings from the experimental results and the scanning electron microscopy with X-ray microanalysis (SEM-EDS) investigation. Chapter 6 concludes the major findings of this thesis and provides some recommendations. Finally, Chapter 7 provides the references used in this thesis.

2 LITERATURE REVIEW

2.1 Carbonates

It is believed that 50% of the world's petroleum reserves are found in carbonate reservoir (Roehl & Choquette, 1985). According to Schlumberger Oil Field Services Carbonate reservoirs contain an estimate of 60% of the oil and 40% of gas reserves of the world (Schlumberger). Carbonates are non-clastic sedimentary rocks that are either formed by biological organisms or chemical precipitation. Unlike sandstones, which are formed externally by weathering of pre-existing rocks, carbonates are mainly formed in-situ on ocean floor from skeleton of organisms and precipitation of sea water that is rich in calcite, aragonite or/and dolomite, and the formation of carbonates is temperature, salinity and substrate dependent (Moore, 2001). Therefore, they are mostly found in warm tropical marine environments. Carbonates are classified into limestone and dolomite based on their mineral composition. Calcite is the primary mineral in limestone while dolomite is the primary mineral in dolomite.

Craze (1950) clearly stated the main difference between limestone and sandstone in terms of their formation characteristics. The geometry of the porous system in sandstone is completely governed by the openings created during deposition. In limestone, however, the shapes and distribution of pore sizes are not uniformly distributed due to secondary solution, recrystallization and fracturing (Craze, 1950).

Chalk is categorized as a limestone due to its high calcite mineral content. It is formed in the open sea (pelagic), has high porosity and low permeability. North Sea chalks are characterized as fractured, overpressured and highly porous. The porosities ranges up to 50% and the matrix permeabilites are considerably low ranging 1-10mD (Lykke, 2005). Fig. 2.1 shows SEM image of Mons chalk.

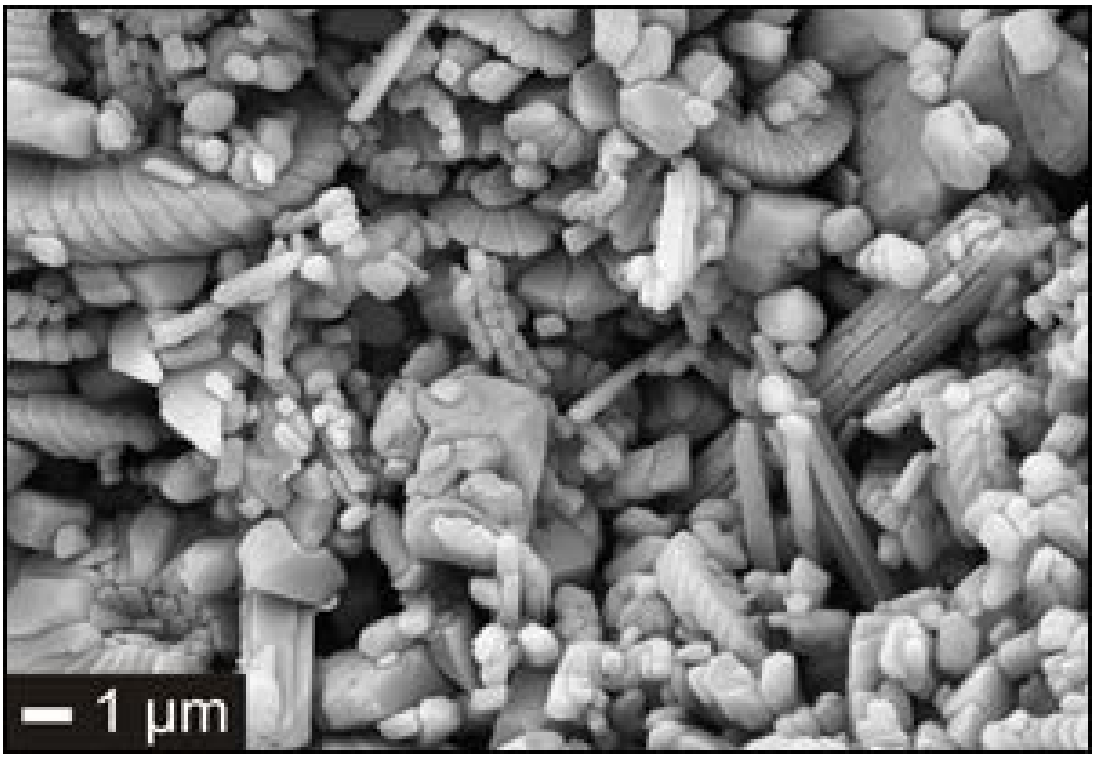

Figure 2.1: SEM image of Mons Chalk (Image taken by Tania)

2.2 Matrix/Fracture Model developed by Anderson & Evje (2012)

Anderson & Evje (2012) had developed a mathematical model which describes the role of spontaneous imbibition as a recovery mechanism in naturally fractured reservoirs where water injection is used. Their model importantly describes the transport mechanism of fluids injected in fractured reservoirs, such as Ekofisk. One of the conclusion drawn from their model was that the importance of the wetting state of the surrounding matrix for imbibition of flooding fluid into the matrix. They clearly concluded that if the flooding fluid was travelling through fracture and the surrounding matrix is oil-wet, only small amount of fluid will imbibe into the matrix. However, if the fracture was surrounded by water-wet matrix, high amount of water will imbibe into the matrix.

2.3 The Ekofisk Field

The Ekofisk field is one of the oldest oil fields in the Norwegian sector of the North Sea, and the field covers an area of 12,000 productive acres and average thickness of

600 feet. It is comprised of two overpressured, naturally fractured and low permeability chalk formations, the Ekofisk and the Tor (Hallenbeck, Sylte, Ebbs, & Thomas, 1991) . The Ekofisk formation was deposited during Palaeocene period and it contained two third of the original oil in place (6.4 billion barrels) and solution gas (10.3 TSCF), with porosities ranging from 25-48 percent and initial water saturation of below 10 percent. The Cretaceous period of Tor formation mainly composed of chalk sediments of Maastrichtian age with porosities between 25 and 40 percent and up to 500 feet oil bearing sections (Hallenbeck et al., 1991; Sylte, Thomas, Rhett, Bruning, & Nagel, 1999).

Sylte et al. (1999) reported that the measured average surface subsidence rate at Ekofisk is 33cm per year and by year 1998 cumulative seafloor subsidence of 7.8 meters had occurred since the beginning of oil production in 1971. It is quite clear that reservoir compaction is the reason behind the Ekofisk field seafloor subsidence. However, what were not clearly understood were the reasons why the compaction was happening. In 1980's it was perceived the compaction was due to reservoir pressure depletion only and the industry thought water injection, for pressure support, would significantly reduce the compaction rate. Although water injection started in 1980's, full scale reservoir management program was launched in 1994 to balance the reservoir pressure using increased water injection , hoping it would reduce the compaction rate. However, the compaction rate was as significant as before the water injection program was implemented. This led to an important conclusion that not only pressure depletion but also the water, which is injected for pressure maintenance, is one of the reasons for compaction. The water was weakening the chalk due to water-chalk surface interaction which can give room to additional compaction.

2.4 Water Weakening Effect on Chalk Reservoirs

Water injection of carbonate reservoirs has been a normal secondary pressure maintenance method in depleted reservoirs. High salinity brines such as sea water or formation water have been used as the injected brines due to their abundance and availability. Numerous experimental studies have been studied to understand the

effect of the ion interaction between high-salinity injected brines, reservoir fluids and rock surface. The strength of chalk decreases as injected water occupies the pore space by displacing the oil originally in place, the phenomenon is known as water weakening (Korsnes, 2007; M. Madland et al., 2008; Risnes, 2001; Risnes & Flaageng, 1999; Risnes et al., 2003). Water weakening effect is one of the causes of reservoir compaction, which can result in higher oil recovery as well as reservoir subsidence.

Austad et al. (2008) pointed out that sea water and chalk interaction at high temperatures has an impact on oil recovery and mechanical properties of the chalk. The ions present in sea water ($Ca^{2+,}$ Mg^{2+}, and SO_4^{2-}) are the determining parameters on the surface chemistry of chalks at high temperature. Two phenomena were observed due to the injection of sea water at high temperatures as a result of wettability alterations: an increase oil recovery by spontaneous imbibition of sea water as well as compaction of chalk which may be due to substitution and adsorption effects at the rock surface. The compaction could also contribute to drive mechanism for oil recovery.

In Korsnes et al. (2006) the mechanical tests performed at 130^{o}C showed that cores flooded with sea water exhibit about 120% higher strain than cores flooded with distilled water during the creep phase at the same stress conditions. This led them to an important conclusion that water weakening of carbonates was not only governed by the mechanical nature of the rock but also the chemical interaction between the pore fluid and chalk surface. They suggested substitution of Ca^{2+} with Mg^{2+} ions and dissolution of chalk explains the temperature effect on the mechanical behavior of the chalk.

Madland et al. (2011) pointed out that the effect of seawater-like brines not only seen during the hydrostatic loading phase but also additional deformation was observed after the chalk has been left to creep. It was hypothetically perceived that magnesium substitutes calcium with the help of sulfate. Contrary to the results reported in Korsnes et al. (2006) which is the presence of sulfate in seawater will lower the strength of chalk, Madland et al. (2011) experimental work demonstrated without the presence of sulfate comparable amount of deformation was observed

and pointed out the possibility of substitution without the presence of sulfate. They suggested substitution process is not the only reason for deformation rather precipitation of magnesium forms new minerals and in this precipitation process both calcite and silicates are dissolved, which results higher deformation because of significant amount of calcite and silicate are dissolved from the rock matrix.

Hedegaard & Graue (2011) performed geomechanical tests using hydraulically operated triaxial tests at ambient temperature to study the impact of wettability alteration on the strength of a chalk. In theory, fully water saturated water wet chalk has lower strength than fully oil saturated water wet chalk as there probably be part of chalk surface which has a stronger preference for oil. However, their experimental results showed the opposite of what they initially assumed. The samples with changed wettability showed lower strength compared to fully water saturated water wet outcrop chalks.

Megawati et al. (2012) presented that the negative surface charge, resulted from adsorption of sulfates to calcite surface, could give rise to a total disjoining pressure which can be the reason for alteration of the mechanical properties of the chalk. They argued, based on their experimental observation, anhydrite precipitation and calcite dissolution were not the case for change in the mechanical properties of the chalk.

As presented above, still some amount of work remain in order to understand the complex chemistry of fluid-chalk surface interaction and it has been difficult to reach in to a certain conclusion on the reasons behind water weakening. Substitution processes, dissolution of chalk and disjoining pressure have been reported as mechanisms behind water weakening effect during water injection. In addition, temperature have been known as one of the main factors that triggers fluid-chalk surface chemical reaction and it should not be taken for granted when performing triaxial mechanical tests.

2.5 Theories of Chalk-Fluid Interactions

Chalk-fluid interaction, by many references, is considered as the driving force behind water weakening effects during water injection. Three main mechanisms have been proposed for chalk-surface interactions: 1) Physical, 2) chemical or 3) physio-chemical (Gutierrez, Oino, & Hoeg, 2000). Here, physical and chemical mechanisms will be discussed.

2.5.1 Capillary Effects

Ahmed (2001) defined capillary forces as " the combined effect of the surface and the interfacial tensions of the rock and fluids, the pore size and geometry, and the wetting characteristics of the system". The discontinuity that arises been two immiscible fluids results a pressure difference between these two fluids and it is known as capillary pressure. Capillary forces have been accounted as one of the mechanisms for chalk-surface interactions. Cohesive force between chalk grains arises at low water saturations since the water that is bounded inside the pore spaces binds the grains together by acting like a bridge (see fig. 2.2). Introduction of more water would fill the voids and results in the collapse of the water brides as well as the capillary forces that bind the grains together. However, the introduction of non-wetting fluids, such as oil, does not destroy the capillary bonds and therefore the water bridges will provide strength for the rocks (Gutierrez et al., 2000).

Other water miscible fluids, such as methanol, have the same effect as water on eliminating the capillary forces created by the water bridges. Since methanol is water miscible, the introduction of methanol in the core sample will likely eliminate the capillary forces. However, in Risnes & Flaageng (1999) work, methanol saturated core samples were much stronger than water saturated samples. This led them to conclude that capillary forces are not the only mechanism of water weakening and that the types of fluids present in the pores have a lot to say.

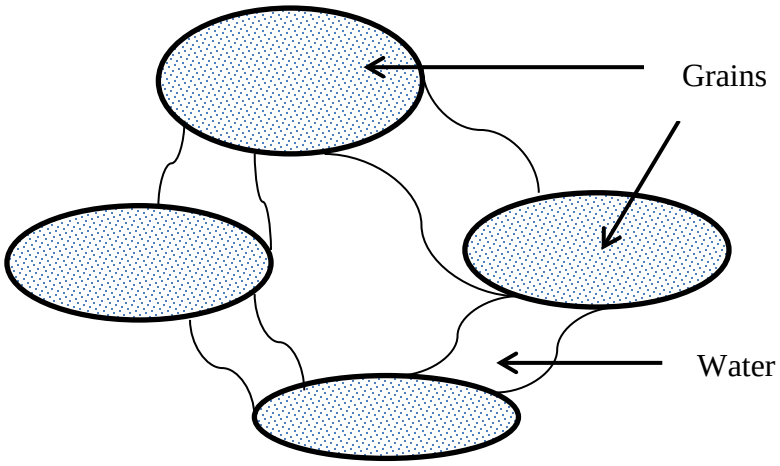

Figure 2.2: The capillary force that is resulted because of the water bridges binds the grains together (Risnes & Flaageng, 1999)

2.5.2 Chemical Effects

The other mechanism that is proposed as one of the mechanisms for water weakening of reservoir chalks is the interaction of chalk surface with the injected chemicals during water flooding. The non-equilibrium state between the pore fluid and rock give rise to dissolution of $CaCO_3$, substitution of Ca^{2+} by Mg^{2+} and precipitation of $CaSO_4$, $SrSO_4$ and $BaSO_4$ depending on the reservoir temperature (Puntervold & Austad, 2007). Dissolution of $CaCO_3$ occurs when the chalk comes in contact with pore fluids, creating additional pore space which can significantly affect the strength of the chalk. Not only dissolution, substitution of Ca^{2+} by Mg^{2+} could also affect the strength of the chalk as Mg^{2+} ion is smaller in size than Ca^{2+}. Puntervold & Austad (2007) summarizes the chemical reactions that could happen when the chalk is in contact with pore fluids:

Reactions related to chalk dissolution:

$$\mathrm{CaCO_3(s)} \Leftrightarrow Ca^{2-} + CO_3^{2-} \tag{2.1}$$

$$CO_3^{2-} + H_2O \Leftrightarrow \mathrm{H}CO_3^{-} + OH^{-} \tag{2.2}$$

$$\mathrm{H}CO_3^- + H^+ \Leftrightarrow H_2CO_3 \quad (2.3)$$

$$H_2CO_3 \Leftrightarrow CO_2(aq) + H_2O \quad (2.4)$$

$$H_2O \Leftrightarrow H^+ + OH^- \quad (2.5)$$

Substitution Reactions:

$$\mathrm{CaCO_3(s)} + Mg^{2+} \Leftrightarrow MgCO_3 + Ca^{2+} \quad (2.6)$$

$$2\mathrm{CaCO_3(s)} + Mg^{2+} \Leftrightarrow CaMg(CO_3)_2(\mathrm{S}) + Ca^{2+} \quad (2.7)$$

Eqn. (2.6) is related to surface substitution reaction and Eqn. (2.7) is related to dolomite formation.

Precipitation Reactions:

$$\mathrm{Ba^{2+} + SO_4^{2-} \Leftrightarrow BaSO_4(S)} \quad (2.8)$$

$$\mathrm{Sr^{2+} + SO_4^{2-} = SrSO_4(S)} \quad (2.9)$$

$$Ca^{2+} + \mathrm{SO_4^{2-} \Leftrightarrow CaSO_4(S)} \quad (2.10)$$

2.6 Mechanical Properties

This section is based on the book “Petroleum related rock mechanics” Fjær (2008) to define terms and explain the theory of rock mechanical properties.

Elasticity is the ability of materials to resist and recover from deformations produced by applied force. Stress and strain are the two concepts that describe the theory of elasticity and they are defined in the following sections. In solid mechanics, the theory of elasticity can be described by the applied stress and the resulting strain. However, in rock mechanics, a slight modification has to be made as petroleum bearing rocks are porous and complex to describe their stress-strain behavior. In addition, the poro-elastic response of a rock material not only depend only the applied loading but also the time when the external stress conditions are constant.

2.6.1 Stress

In simple terms, stress is defined as force per unit area of solid material. Stress and pressure are the same parameters except the latter is used to describe the state of fluids. Mathematically, stress is defined as:

$$\sigma = \frac{F}{A} \tag{2.11}$$

Where F is the force acting on the cross sectional area A. The SI unit of stress is Pascal (N/m^2).

To elaborate more, consider the situation in Fig. 2.3 at point a and b. Consider the case at a, the stress is given by the force acting on the cross section per unit area, $\sigma = F/A$. If the cross sectional area is smaller, the stress will be larger. This means the magnitude of stress is position dependent and it varies according to the area along different positions in the material.

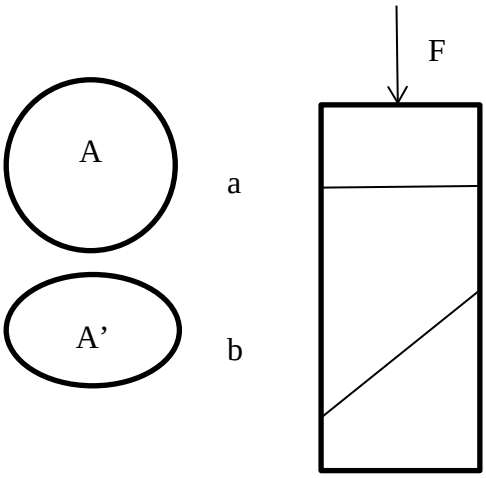

Figure 2.3: Illustration of Forces and Stresses

The condition at point b shows the importance of the orientation of the cross section relative to the direction of the force. Consider the situation in Fig. 2.4, at point b, where the force is no longer perpendicular to the cross section. The force can be taken as a resultant force and decompose into two forces; one component (F_n) normal to the surface and another one component (F_p) parallel to the surface (see Fig. 2.4). The two component forces produce two completely different stresses and are quantified as:

$$\sigma = \frac{F_n}{A'} \tag{2.12}$$

$$\tau = \frac{F_p}{A'} \tag{2.13}$$

The stress produced by the normal force is known as *normal stress* and, likewise, the stress produced by the force parallel to the cross section is known as *shear stress*.

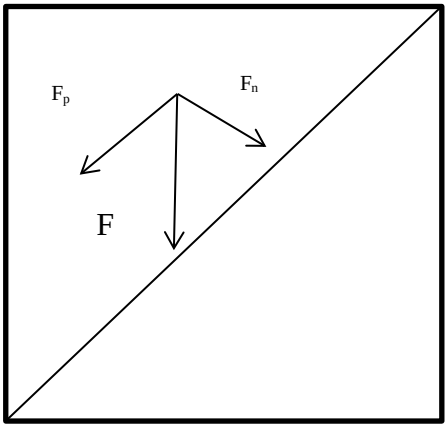

Figure 2.4: Decomposition of resultant force into component forces

A stress state at a point in a given sample should be described based on the stresses related to the orientation of the surface in three orthogonal directions. The stresses $\sigma_x , \tau_{xy} , \tau_{xz}$ are related to surface normal to the x-axis. Likewise, the stresses $\sigma_y , \tau_{yx} , \tau_{yz}$ are related to surface normal to the y-axis, whereas $\sigma_z , \tau_{zx} , \tau_{zy}$, are related to surface normal to the z-axis. As a convention, the first index in the notation is associated with the face normal while the second index shows the direction of the force. For instance, the notation σ_x represents a stress related to surface normal to x-axis, τ_{xy} represents the shear stress where the direction of the force is in y-direction, and τ_{xz} represents the shear stress where the direction of the force is in z-direction. Therefore, there are nine independent stress components at a given point within a sample and are described as *stress tensor* and is denoted by $\overleftrightarrow{\sigma}$.

$$\overleftrightarrow{\sigma} = \begin{pmatrix} \sigma_x & \tau_{xy} & \tau_{xz} \\ \tau_{yx} & \sigma_y & \tau_{yz} \\ \tau_{zx} & \tau_{zy} & \sigma_z \end{pmatrix} \tag{2.14}$$

The number of independent stress components may be reduced from nine to six for an object at rest. Fig. 2.5 shows the stress acting on a square object in two dimensions. Since the object is at rest there is no net rotation or translation of the object. Therefore, the following must be true for no rotation:

$$\tau_{xy} = \tau_{yx} \tag{2.15}$$

$$\tau_{xz} = \tau_{zx} \tag{2.16}$$

$$\tau_{yz} = \tau_{zx} \tag{2.17}$$

By using the three equations above, the stress tensor can be re-written as:

$$\overleftrightarrow{\sigma} = \begin{pmatrix} \sigma_x & \tau_{xy} & \tau_{xz} \\ \tau_{xy} & \sigma_y & \tau_{yz} \\ \tau_{xz} & \tau_{yz} & \sigma_z \end{pmatrix} \tag{2.18}$$

To minimize the ambiguity using different notations for normal and shear stress and for practical purposes, both normal and shear stresses are denoted by σ_{ij}. The subscripts i and j denote numbers from 1, 2 and 3, which represent the Cartesian coordinates x-axis, y-axis and z-axis, respectively. Finally the stress tensor, where the symmetry of the stress tensor is used, can be written as:

$$\overleftrightarrow{\sigma} = \begin{pmatrix} \sigma_{11} & \tau_{12} & \tau_{13} \\ \tau_{12} & \sigma_{22} & \tau_{23} \\ \tau_{13} & \tau_{23} & \sigma_{33} \end{pmatrix} \tag{2.19}$$

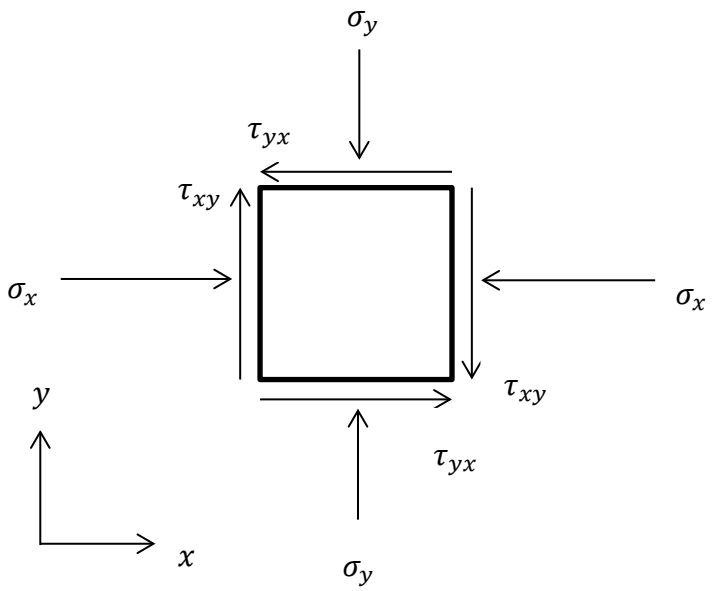

Figure 2.5: Stress Components in two dimensions

2.6.2 Principal Stresses

There exists orientation of coordinate system where all the shear stresses vanish. The non-zero normal stresses are called principal stresses and the directions are known as principal axes. However, one has to put in mind that the state of stress condition within the given sample would be the same although the shear stresses vanish. Here, we only focus on stresses in two dimensions. Fig. 2.6 shows the normal (σ) and shear stress (τ) for the surface normal to an arbitrary θ direction in xy-plane. If we assume the triangle in Fig. 2.6 is at rest, the net force normal and parallel to the surface will be zero. Therefore, equilibrium of forces implies:

$$\sigma = \sigma_x \cos^2\theta + \sigma_y \sin^2\theta + 2\tau_{xy} \sin\theta \cos\theta \tag{2.20}$$

$$= \frac{1}{2}(\sigma_x + \sigma_y) + \frac{1}{2}(\sigma_x - \sigma_y)\cos 2\theta + \tau_{xy} \sin 2\theta \tag{2.21}$$

$$\tau = \sigma_y \sin\theta \cos\theta - \sigma_x \cos\theta \sin\theta + \tau_{xy} \cos\theta \cos\theta - \tau_{yx} \sin\theta \sin\theta \tag{2.22}$$

$$= \frac{1}{2}(\sigma_y - \sigma_x)\sin 2\theta + \tau_{xy}\cos 2\theta \quad (2.23)$$

Choose θ so that the shear stress (τ) becomes zero, and this happens when:

$$\tan 2\theta = \frac{2\tau_{xy}}{\sigma_x - \sigma_y} \quad (2.24)$$

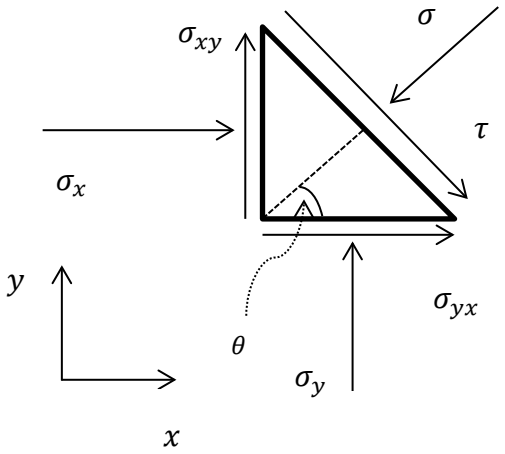

Figure 2.6: Equilibrium of Forces

Solving Eqn. (2.24) gives two solutions, θ_1 and θ_2, which corresponds to two principal directions that the shear stress (τ) disappears. Since we have two solutions, θ_1 and θ_2, we will have two principal normal stresses σ_1 and σ_2 which correspond to each principal axis. The two principal stresses are calculated by substituting θ_1 and θ_2 into Eqn. (2.21).

2.6.3 Strain

It is important to measure the deformation of a given sample after a force is applied to it. Apparently, a material would be compressed if the force was compressive or stretched if the force was tensile. Consider a chalk core sample as shown in Fig. 2.7, which is subjected to axial compressive force F. After the action of the force, the material becomes shorter as all the particles inside the material shift their positions.

The quantity that measures the deformation of the given sample after the action of a force is known as Strain, ε. Mathematically, it is defined as:

$$\varepsilon_a = \frac{L - L'}{L} = \frac{\Delta L}{L} \tag{2.25}$$

Where ε_a is the axial strain, L is the length of the original material and $L'$is the length after the action of the force.

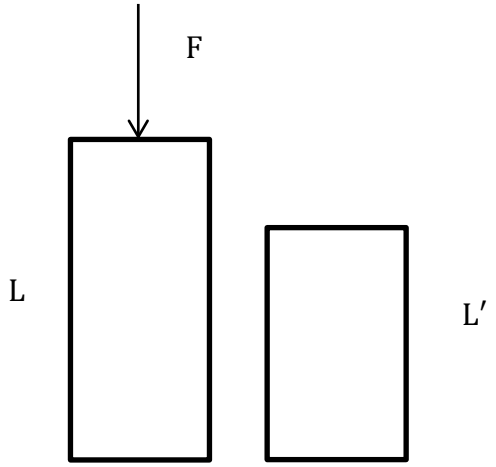

Figure 2.7: Deformation of a material after the action of force

Needless to say, if the material is subjected to force which acts radial, the radial strain is given as:

$$\varepsilon_r = \frac{D - D'}{D} = \frac{\Delta D}{D} \tag{2.26}$$

Where ε_r is the radial strain, D is the diameter of the material before deformation and D' is the diameter after deformation.

Most often engineering problems deals with materials which are under axial and radial forces and therefore it follows the need to measure the deformation volumetrically. The volumetric strain for a given sample is defined as:

$$\varepsilon_v = \varepsilon_a + 2\varepsilon_r \tag{2.27}$$

For isotropic material where all the forces acting in different direction are equal, Eq. (2.17) can be re-written as:

$$\varepsilon_v = 3\varepsilon_a = 3\varepsilon_r \tag{2.28}$$

2.6.4 Stress-Strain Relationship

As stated in section 2.6.3, strain is a measure of the response of a given sample that has been under stress. It is straightforward to understand the nature of the relationship between stress and strain. The higher stress we apply on to a material, higher strain is measured. Therefore, for elastic materials, stress is directly proportional to strain and can be put mathematically as follows:

$$\sigma \; \alpha \; \varepsilon \tag{2.29}$$

To complete the mathematical description, proportionality constant should be included in to Eqn. (2.29). The type of the proportionality constants vary based on the type of loading. For hydrostatic loading, where all the stresses in all directions are equal, the proportionality constant K is introduced. For deviatoric tests, the proportionality constant E is introduced. Where K is bulk modulus of elasticity and E is Youngs modulus of elasticity. Therefore, the stress-strain relationship can be written as:

$$\sigma = E\varepsilon \tag{2.30}$$

$$\sigma = K\varepsilon_v \tag{2.31}$$

Eqn. (2.30) and Eqn. (2.31) are different forms of *Hook's law* depending on whether the test is deviatoric or hydrostatic, respectively.

Fig. 2.8 depicts the graphical representation of strain-stress relationship. At the origin there is no stress and strain in the test sample. Up to the elastic limit, the stress is directly proportional to the strain and obeys Hook's Law. The curve between the elastic limit and the yield point is not a straight line and strain increases faster than stress beyond the elastic limit. The yield point is the point after which stress results permanent deformation. Beyond the plastic limit, failure is start to initiate and material completely fails when it reaches its ultimate stress.

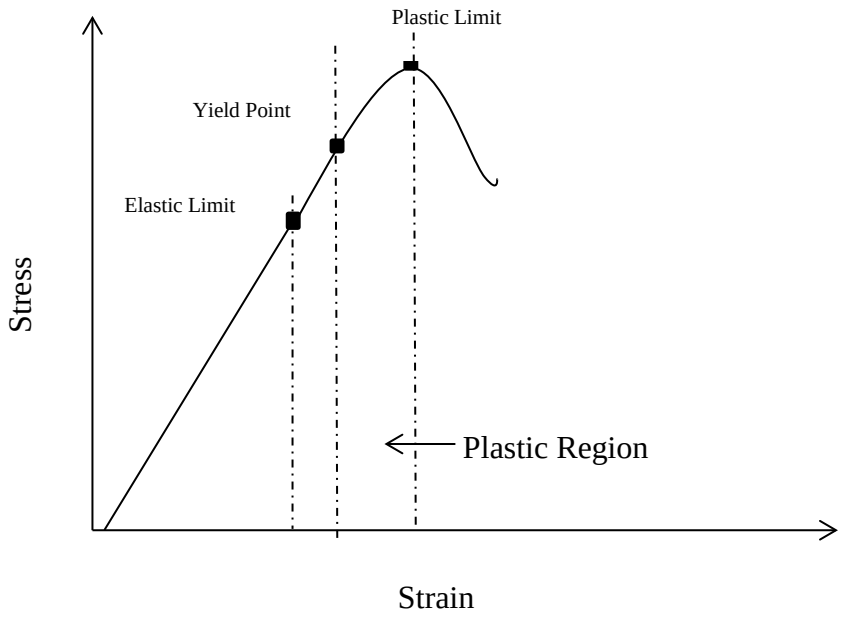

Figure 2.8: Stress-Strain Relationship Curve

2.6.5 Creep

In section 2.6.4, we assumed that for every stress applied to rocks there is an immediate response of deformation. However, this is not always true since laboratory experiments showed deformation of rocks continues for long time after a change in the applied stress. Fjær et al. (2008) divided this time dependent effects in to two groups: *consolidation* and *creep*. Consolidation results when there is a disturbance of pore pressure equilibrium due to change in applied stress, and it takes time to re-establish the equilibrium. Creep is time dependent deformation that results under constant stress. Fig. 2.9 shows the three different stages of creep: *transient*

(primary), *steady state (secondary)* and *accelerating (tertiary) creep*. During transient creep stage the time dependent deformation decreases with time and the deformation is dependent on the applied constant stress. If the applied stress is reduced to zero, the creep eventually becomes zero. During the steady state creep, the rate of deformation is constant. Steady state creep implies a permanent deformation of materials since the deformation will not be zero if the applied stress is reduced to zero. During the accelerating creep stage, the rate of deformation increases with time.

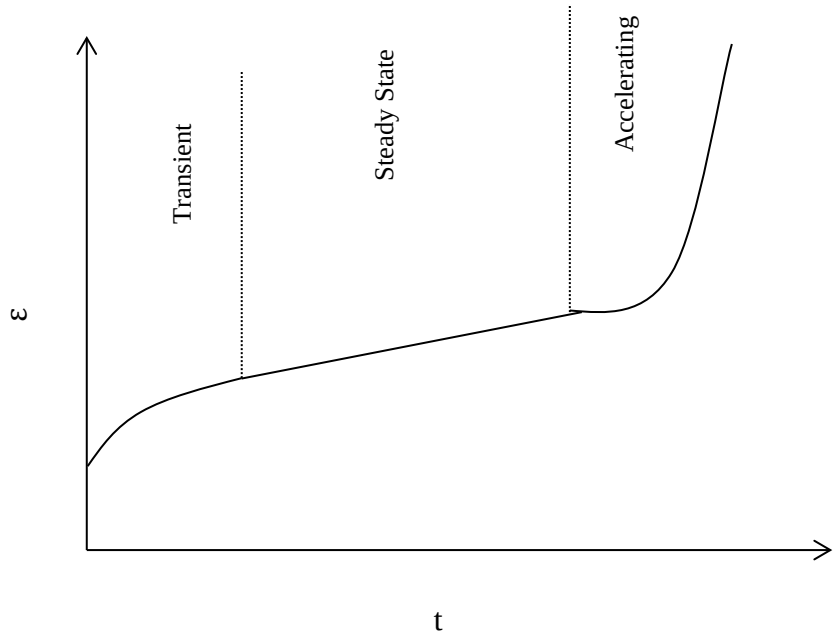

Figure 2.9: The three stages of Creep (Fjær et al. 2008)

2.6.6 Creep Strain Rate

The creep strain rate, m, is an important parameter that can be used to measure how the strain develops through time. It is specially used when there is a need to measure the strain rate during creep phases by plotting axial strain versus the logarithm of time. A linear trend line can be added to the logarithmic plot and the creep strain rate can be calculated using the following equation.

$$m = \frac{\Delta \varepsilon_c}{\Delta log t} \tag{2.32}$$

Where ε_c is creep strain [%] and t is creep time [days]

3 METHODOLOGY

3.1 Test Material and Preparation

The core samples used throughout this work has been cored, in the laboratory, from outcrop chalk. The outcrop chalk was collected from the Obourg quarry at Saint Vast near the town of Mons, Belgium. The chalk is characterized by high porosity, ranging 40-42%, and low permeability. All the core samples used for the experiments were labeled as Obourg Saint Vast (OB SV) and followed by a number.

After the samples were cored from the outcrop block, Lathe machine was used to shape, polish and drill 2 mm hole, to introduce fracture, at the center of the core samples. Diamond cutter was used to cut the samples to the desired dimensions.

The initial porosities were calculated based on normal laboratory procedure which is weight analysis. The samples were dried in the heating chamber above the boiling point of water to make sure all the water was evaporated. Then the samples were vacuumed to approximately 0.04 kPa before they were saturated with distilled water. Both the dry and the fully saturated weight of the cores were measured. The porosities then calculated based on these two weights. The equations used for calculating porosities are as follows:

$$Pore\ Volume\ (PV), cm^3 = \frac{W_{wet} - W_{dry}}{\rho_{Brine}} \quad (3.1)$$

$$Bulk\ Volume\ (BV), cm^3 = Area\ [cm^2] * Length\ [cm] \quad (3.2)$$

$$Porosity\ (\emptyset), \% = \frac{PV}{BV} * 100 \quad (3.3)$$

3.2 Summary of Equipments

Different equipments were used for core sample preparation, pumping of fluids, chemical analysis and mechanical loading of the core samples. All the mechanical tests for this thesis were performed on hydraulically operated triaxial cells (Fig. 3.1). The cells were equipped with three high pressure pumps which provide confining pressure, axial pressure and pore pressure. Linear Voltage Displacement Transducer (LVDT) was attached with the cells to measure axial displacement in real time. It is worth noting that no radial displacement was measured as there was no radial measuring device attached with the cells. LabView computer software was used to log all real time data recorded from the experiments. In addition, the cells were equipped with a heater, Backer 1500W heating Jacket, to increase the temperature of the cells to 130℃. The detailed triaxial cell description and design can be referred to the Doctoral Dissertation of Omdal (2010).

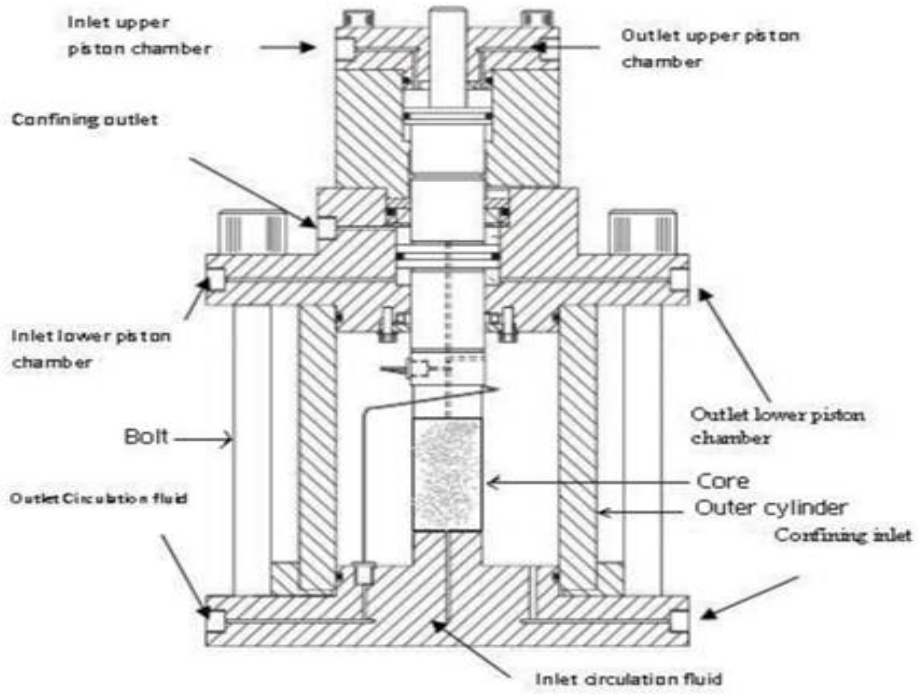

Figure 3.1: Triaxial Cell. Details of triaxial cell used

3.3 Chemical Analyses

Water samples were taken throughout the experiments to analyze and compare the ion concentration of the produced fluid with the injected fluid. The original injected fluid ion concentrations were taken as a standard during the analysis. Dionex ICS-3000 Ion Chromatography system (Fig. 3.2) was used for the chemical analysis. The system offers the capability of analyzing cations and anions separately. The following simple steps were taken for the chemical analyses:

- Dilute the water samples 500 times using Gilson Gx-271.
- Filter the diluted samples using syringe and a filter.
- Run the chemical analysis using Dionex ICS-3000 Ion Chromatography System.

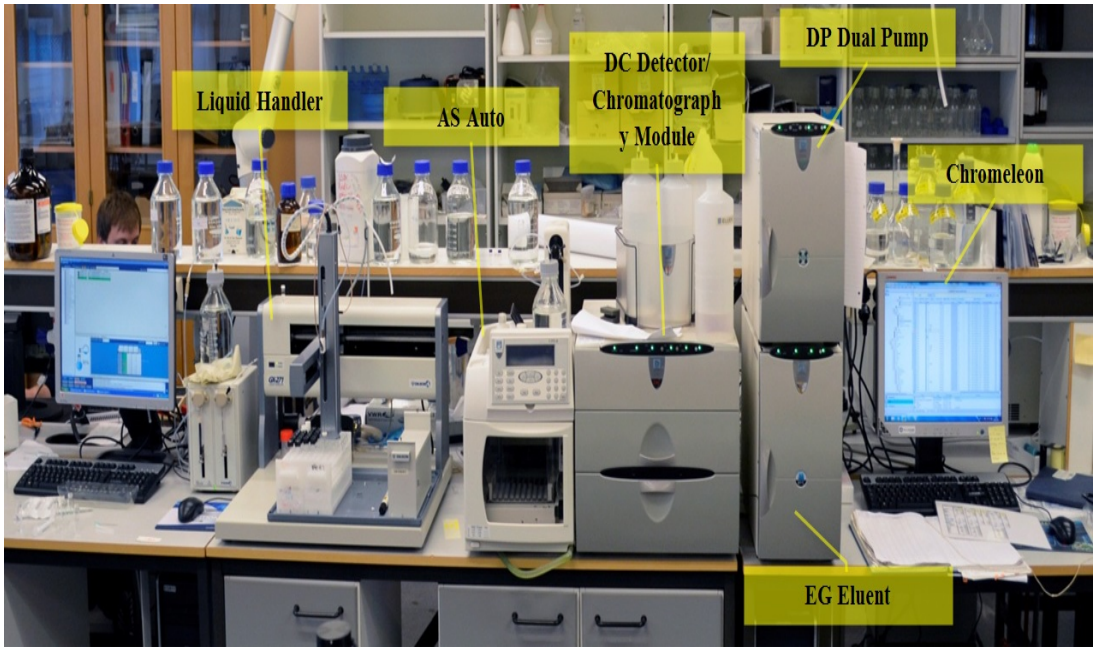

Figure 3.2: Dionex ICS-3000 Ion Chromatography system. It is used for chemical analysis

3.4 Fluids

Five various types of fluids were mainly used during the course of the experimental work to clean, saturate or flood the core samples. The brines were prepared in the laboratory based on normal laboratory procedure. Table 3.1 lists the different fluids with their composition and purpose.

Table 3.1: Various fluids' purpose and composition

Brine	Purpose	Composition
Distilled Water (DW)	Used to clean, saturate cores. Were used as well to flood	Water without any impurities
Sodium Chloride Brine NaCl	Used to saturate and flood the cores for creep experiments	0.657 M NaCl
Synthetic Sea Water SSW	Used for Creep experiments	NaCl=23.38g/mol, Na_2SO_4=3.41g/l, $NaHCO_3$=0.17g/l, KCl=0.75g/l, $MgCl_2$+6H_2O=9.05/l, $CaCl_2$+2H_2O=1.91g/l
Magnesium Chloride Brine $MgCl_2$	Used for Creep experiments	0.219 M $MgCl_2$

3.5 Experimental Procedure

Before the triaxial test was started the core sample was saturated with 0.657M NaCl brine to make sure all the pore spaces were invaded with the brine. The sample then was installed in to the triaxial cell and the confining pressure was increased to 0.5MPa to prevent leakage as well as prevent the saturation brine (in this case

0.657M NaCl brine) out of the core when we start flooding. Then the core sample was flooded with the same brine for approximately a day. During the second day, the pore and confining pressure were increased to 0.7 and 1.2 MPa, respectively. The temperature of the cell was increased to 130℃, to simulate the reservoir temperature condition at Ekofisk field, using Backer 1500W heating Jacket. In the same day the piston pressure was increased to 0.7MPa (frictional pressure 0.4MPa and piston pressure 0.3MPa). Once the desired confining and pore pressure was reached, the core was flooded with a rate of one pore volume per day (1 PV/Day). During the third day, the hydrostatic test was started by increasing the confining pressure to 12MPa (to load the cores beyond the yield point). To prevent a sudden failure, the confining pressure was increased very slowly with a rate of 0.05ml/min. Once confining pressure of 12MPa was reached, the core was left to creep for the rest of the experimental phase. During the creep phase, however, after approximately six days the type of injected bring was switched from 0.657M NaCl brine to synthetic sea water (SSW) or 0.219 M $MgCl_2$ depending on the type of brine used. The following steps explain the detailed experimental procedure:

Day one

- Saturate the core sample with 0.657M NaCl brine. The sample was vacuumed up to 0.04KPa before saturation started.
- Install the core in to the triaxial cell. The sample was mounted on the base of the cell. The sample then was covered with a plastic sleeve and the sleeve was heated to attach it on the body of the sample. This was done to give extra protection for the core. The steel cylinder then was mounted on the outer base of the cell and hydraulic oil was filled between the core and the steel cylinder. Finally the cell was bolted and LVDT was placed on the top of the cell for axial measurement.
- Increase the confining pressure to 0.5MPa. This helps to prevent any leakage as well as prevent brine out of the core. The confining pressure was increased using the high pressure pumps through the hydraulic oil inside the cell.
- Start flooding the core with 0.657M NaCl brine for a day. The normal flooding rate for the experiments was one pore volume per day (1PV/day).

The flooding was done using flooding cell that is attached with a pump. The flooding cell has two chambers; one for distilled water and another one for injected brines. A piston is placed between the chambers to push the brines in to the core.

Day Two

- Increase the pore and confining pressure to 0.7 and 1.2MPa, respectively. The pore pressure was increased to prevent boiling when the temperature was raised to 130℃. .
- Increase the temperature to 130℃. The confining pressure was kept 1.2MPa using pressure regulating valve as increasing temperature would effectively influence the confining pressure.
- Increase the piston pressure to 0.7MPa.

Day 3 and the rest of the days:

The hydrostatic Test

- Increase the confining pressure to 12M. To prevent failure, the flooding rate was set to 0.05ml/m.
- Set the piston pressure between 0.7 and 0.9 MPa.

Creep Phase

- Once confining pressure of 12MPa was reached (to load the core beyond yield point), the core was left to creep for the rest of the experimental days. After approximately six days, type of brine was changed from NaCl brine to 0.219M MgCl2 or synthetic seawater (SSW) depending on the type of experiment.

3.6 Porosity Calculations

After the mechanical tests, the cores were dried using a heating chamber and the dry weight of the cores were measured. Then, the cores were cut in to 6-7 slices (see Fig 3.3) and the weight of each slice was measured. Finally, the volume of each slice was measured by using Gas Pycnometer (See Fig 3.4) in order to determine the average density of the cores.

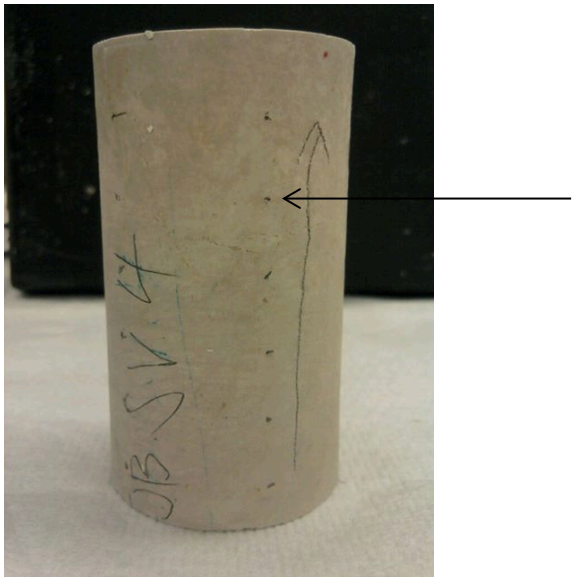

Figure 3.3: Core sample OB SV 4 after the mechanical test

Porosity calculations were made to compare the original porosity of the cores with the porosity of the cores after the mechanical tests. Two approaches were used to calculate the porosities; 1) mechanical porosity calculation without considering the chemical alterations that might occur during the creep experiments. 2) Porosity calculations which consider both the mechanical and chemical effects on the core.

Figure 3.4: Gas Pycnometer was used to measure the volume of the cores. Based on the volume measured and the weight of the cores, the densities of the cores were calculated.

The calculations were made based on the following formulas:

Mechanical Porosity Calculation

$$\phi = \frac{\phi_o - \varepsilon_v}{1 - \varepsilon_v} \tag{3.4}$$

Where ϕ is porosity after test, ε_v is volumetric strain and ϕ_o is initial porosity.

Mechanical and Chemical Porosity Calculation

$$\phi = 1 - \frac{M_s}{\rho V_B} \tag{3.5}$$

Where ϕ is porosity, M_s is solid mass of the core and ρ is density of the core and V_B is the bulk volume.

The volumetric strain was calculated by using the original bulk volume and the bulk volume of the core after the tests as follows.

$$\varepsilon_v = \frac{V_B - V_B'}{V_B} \tag{3.6}$$

Where V_B is the original bulk volume and V_B' is the bulk volume after the mechanical test and. To calculate V_B', each core samples were sliced in to pieces and the average diameters and the heights of each pieces were measure. Then the following formula was used to calculate the new bulk volumes of each core:

$$V_B' = \frac{1}{3}\pi({r_n}^2 * r_n * r_{n+1} * {r_{n+1}}^2) * h \tag{3.7}$$

Where r is the radius of the pieces, n is the pieces' number and h is the height of the pieces.

The average densities of the cores were calculated by taking the weighted average of the densities of each slice as follows:

$$\rho_{av} = \rho_n \frac{v_t}{v_n} + \rho_{n+1} \frac{v_t}{v_{n+1}} + \rho_{n+1} \frac{v_t}{v_{n+2}} + \cdots$$

Where ρ_{av} is average density, ρ_n is the density of the n^{th} slice and v_t is total volume of the core.

4 RESULTS

The experimental works have been done jointly with Geitle (2013) in order to compare and contrast the results obtained. Two triaxial cells were used to test five Mons chalk core samples; OB SV 4, OB SV 6, OB SV 9, OB SV 12 and OB SV 18. Artificial fracture was introduced by drilling two millimeter hole, vertically, in the middle of OB SV 4, OB SV 12 and OB SV 18 core samples. OB SV 6 and OB SV 9 core samples were left as intact. Table 4.1 summarizes the core data that was collected prior to the mechanical tests. The results are presented in to two sections; the first section presents all the intact core samples' results and the second section presents the entire fractured core samples' results.

Table 4.1: Tested Cores' Properties

Core Sample	Wdry [g]	Wwet [g]	L [mm]	D [mm]	BV [cc]	PV [cc]	Porosity [%]
OB SV 4	125.23	156.96	68.81	38.13	78.35	31.72	40.49
OB SV 6	127.65	160.24	70	38.11	79.8	32.57	40.81
OB SV 9	126.57	160.54	70.1	38.13	80	33.072	41.34
OB SV 12	123.56	156.75	68.54	38.12	78	32.25	41.34
OB SV 18	122.94	155.86	68.28	38.09	77,77	32.03	41.18

4.1 Intact Chalk Samples (OB SV 9 and OB SV 6)

4.1.1 Mechanical Tests

The mechanical tests comprised of two distinct parts; the hydrostatic phase and the creep phase. During the hydrostatic phase, the core samples were loaded hydrostatically, beyond their yield point, until the confining pressure reaches approximately 12 MPa (This point was chosen to load the cores 2.5-3MPa beyond the yield point). During this phase all the samples were flooded with 0.657 M NaCl at the rate of 1 pore volume per day (PV/day). Following the hydrostatic phase the samples were left to creep under constant confining pressure of 12 MPa.

4.1.1.1 The Hydrostatic Phase (Intact Cores)

As mentioned above, OB SV 6 and OB SV 9 core samples were left as intact and with the help of Labview computer software the confining pressure, the axial movement of the samples, the pore pressure and the piston pressure were recorded. The axial stress and strain was then calculated based on the recorded data and plotted as shown in Fig. 4.1. The bulk modulus (K), the yield point and the total strain values were found based on the plot. The bulk modulus value was found based on the slope of the linear stress-strain curve in the elastic region. For isotropic materials the bulk modulus is one third of the slope of the linear stress-strain curve. Therefore the K-values were calculated using the slope of the stress-strain curve in the elastic region and Eqn. (2.31). Similarly, the yield point of the core samples was found simply by adding two tangent lines on the curve; one for the elastic region and another one after the elastic region, and the intersection of the two tangent lines were assumed to be the yield point. Table 4.2 summarizes the results during hydrostatic loading for the intact cores.

Table 4.2: Mechanical test Results during hydrostatic loading for the intact cores. The intact cores have shown amazing similarities in yield strength and K-values. This indicates that hydrostatic tests have excellent repeatability.

Core Sample	Porosity [%]	Length [mm]	Yield Strength	K-Value [GPa]	Total axial Strain [%]
OB SV 6	40.81	70	9.6	0.68	0.795
OB SV 9	41.34	70.1	9.4	0.67	0.904

The results show that OB SV 6, with porosity of 40.81% and length of 70 mm, has yielded at 9.6 MPa axial stress, and strained 0.795 % percent of the total length after the hydrostatic loading, and the calculated K-value assuming an isotropic condition was 0.68 GPa. Similarly, OB SV 9, with porosity of 41.34% and length of 70.1 mm, 9.4 MPa yield strength, 0.904 total axial strain and K-value of 0.67 GPa was found. One simply may observe that both the intact cores have shown very similar yield strengths and K-values and it can be deduced that hydrostatic tests are very repeatable.

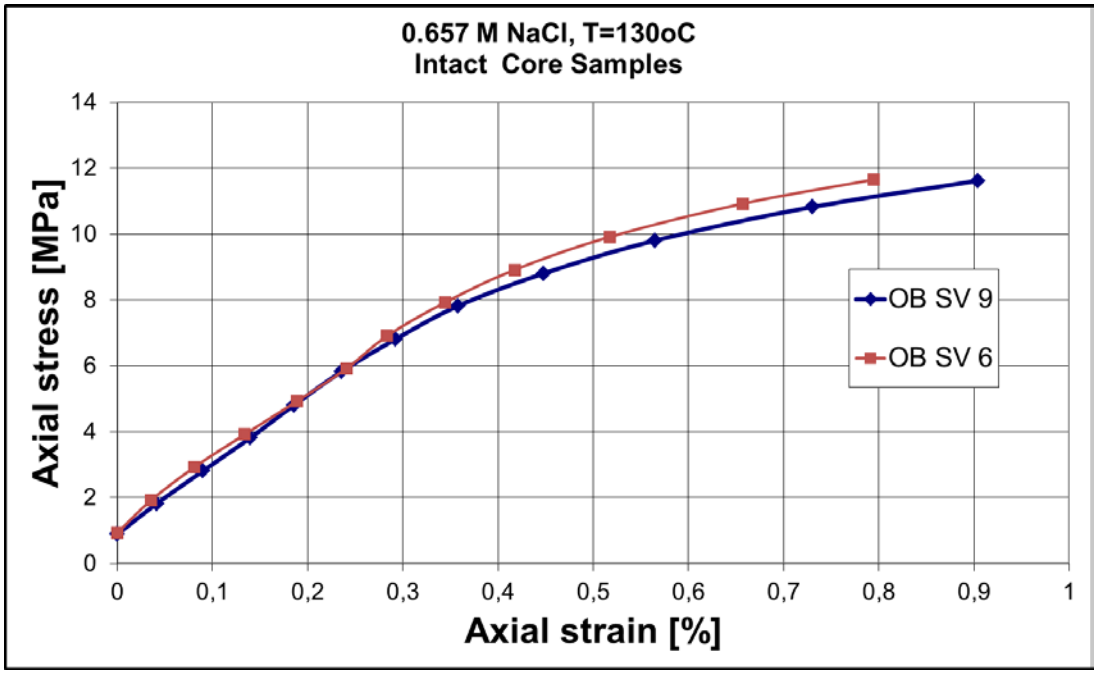

Figure 4.1: Axial Stress [MPa] Plotted as a function of axial strain [%] for the intact cores (OB SV 9 and OB SV 6). The results shows that the yield strength and the K-values are very similar (the yield curves are more or less overlapping)

4.1.1.2 Creep Phase (Intact Cores)

The creep phase of the experiment was started the moment the confining pressure reached 12MPa (which is at the end of the hydrostatic loading phase). During this period constant confining pressure of 12MPa was kept until the end of the test and type of fluid was switched from NaCl to other desired fluids. The total axial strain that was recorded during the hydrostatic loading was not part of the strain that was found during the creep phase. To show the deformation of the core samples under constant stress, axial strain after the hydrostatic loading versus time was plotted in all the experiments. The creep phase results for the intact cores are summarized in Table 4.3. The results presented in Table 4.3 are described in more detail in the following sections.

Table 4.3: Summary of Flooding brine, total axial creep strain and creep strain rates for intact cores. Intact core OB SV 9 was flooded with 0.657 M NaCl brine for six days and followed by SSW for about 15 days. Intact core OB SV 6 was flooded with 0.657 M NaCl brine for six days and followed by 0.219 M $MaCl_2$ brine for about 40 days.

Core Sample	Flooding Fluid	Flooding Periods [days]		Volume Flooded [ml]	Total Axial Creep Strain [%]	Initial Strain rate, [%/decade]	Final Strain rate, [%/decade]	
		Start	Stop					
OB SV 9	NaCl	0	6	198.72	1.06	----	1.61	
	SSW	6	19.83	438.13	2.70	1.25	16.5	9.28
	DW	19.8	21.57	---	2.74	---	---	
OB SV 6	NaCl	0	6	198.78	1.169	---	1.84	
	$MgCl_2$	6	45.96	1323.48	2.45	1.13	6	
	DW	49.96	48.83	---	2.52	---	---	

The Creep Phase; Intact Core OB SV 9 (SSW)

Fig. 4.2 shows the results that were observed during the creep phase for OB SV 9. In addition to the observed results, trend lines were added to further examine the evolution of the creep during the course of the experiment. Also, this is done for the other experiments.

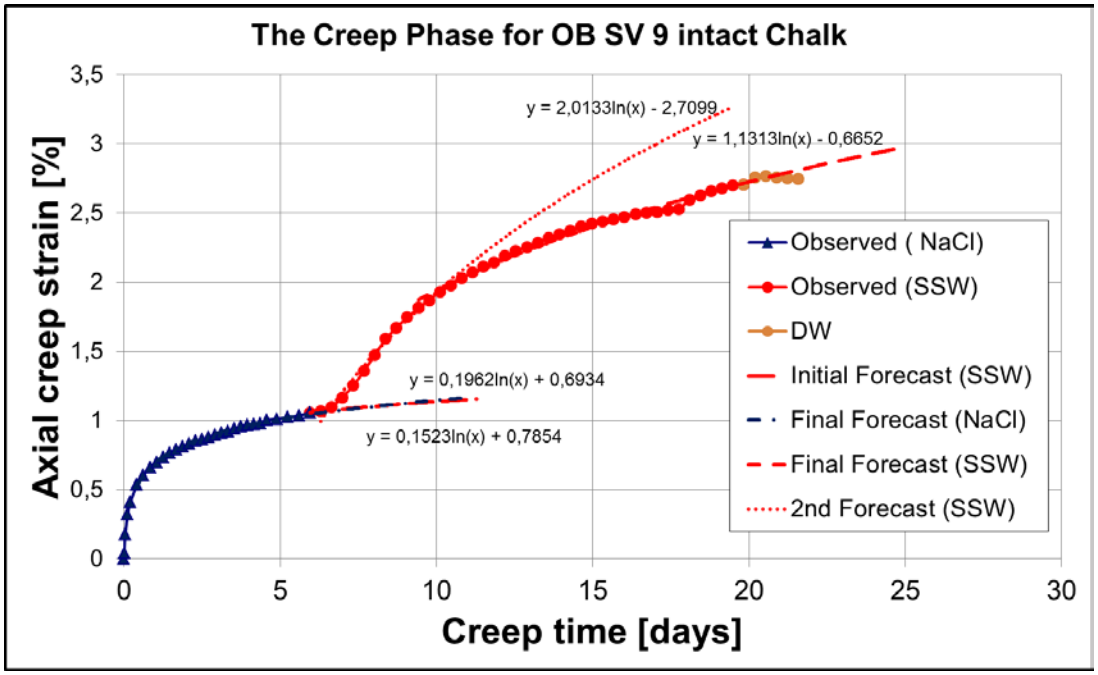

Figure 4.2: Axial Creep Strain [%] as a function of Creep Time [days] for OB SV 9 was plotted. The core was flooded with 0.657 M NaCl for the first six days and the flooding fluid was switched to SSW for another 15 days. Immediately after brine change, it was observed mechanical response of the core.

For the first six days of the creep phase, OB SV 9 was flooded with 0.657 M NaCl and it was switched to synthetic sea water (SSW) for another 14.53 days as shown in Table 4.3. During NaCl flooding, strain rate of 1.61 %/decade was observed. After six days, 1.06% total axial creep strain was observed. If NaCl had been used for the entire test, the creep strain rate would have been only 1.61 %/decade as it was forecasted using logarithmic trend. However, the NaCl brine had been switched to SSW to observe what effect it might have on the creep. It turned out, after the switch it only took about 15 hours to observe the effect of the SSW on the creep although in previous tests the response time was even faster. For the first 15 hours after the switch, the creep strain, 1.25 %/decade, was rather slower than what was observed during the sixth day of NaCl flooding (1.61%/decade). This could be because of time delay that might occur for SSW to reach the core from the pumps. Beyond the 15 hours mark after the switch, the creep strain rate had increased to 16.51 %/decade, which is more than 10 times higher than what was observed during the latter days of NaCl brine flooding (1.61 %/decade). However, the 16.51 %/decade creep strain rate only continued for another three days and after that the creep strain rate started to drop for the final days of the experiment. Final creep strain rate of

9.28 %/decade was observed during SSW flooding. Unfortunately, the test for this core had to be stopped after 20 days since we were not able to flood more fluids as the core was clogged and by this time 2.70% total axial creep strain was observed. Then the core was cleaned with distilled water for about two days and total axial strain of 2.74% was observed after the cleaning. Despite the fact that it had to be stopped, logarithmic forecast was made using the data collected during the last days of the test (see Fig. 4.2).

The Creep Phase; Intact Core OB SV 6 (0.219M $MgCl_2$)

For the first six days of the creep phase, OB SV 6 was flooded with sodium chloride brine (0.657 M NaCl) and it was switched to magnesium chloride brine (0.219 M $MgCl_2$) for another 39.96 days as shown in Table 4.3. As shown on Fig 4.3, during the first six days, similar trends as OB SV 9 were observed for OB SV 6 although the creep strain rates were higher than what was observed for OB SV 9. During these six days, the creep strain rate followed logarithmic trend and the observed value was 1.84%/decade. After six days, total axial creep strain of 1.169% was observed. It would have followed the same trend, if NaCl brine was kept as the flooding fluid as forecasted (see Fig.4.3). However, the flooding fluid was switched to $MgCl_2$ to check if it has got an effect on the creep strain. For approximately three days after the switch, $MgCl_2$ brine had not contributed more than what was observed during the final days of NaCl brine flooding. During this time only about 1.13 %/decade creep strain rate was observed. But it was after these three days, the effect of $MgCl_2$ on the creep started to show up. Final Strain rate of 6 %/decade was observed starting day 9 until the end of the experiment. The final strain rate has increased 5.31 times compared to what was observed during the initial three days of $MgCl_2$ flooding. After approximately 46 days, total axial creep strain of 2.45% was observed. Then the core was cleaned for about three days and total axial creep strain of 2.52% was observed after the cleaning.

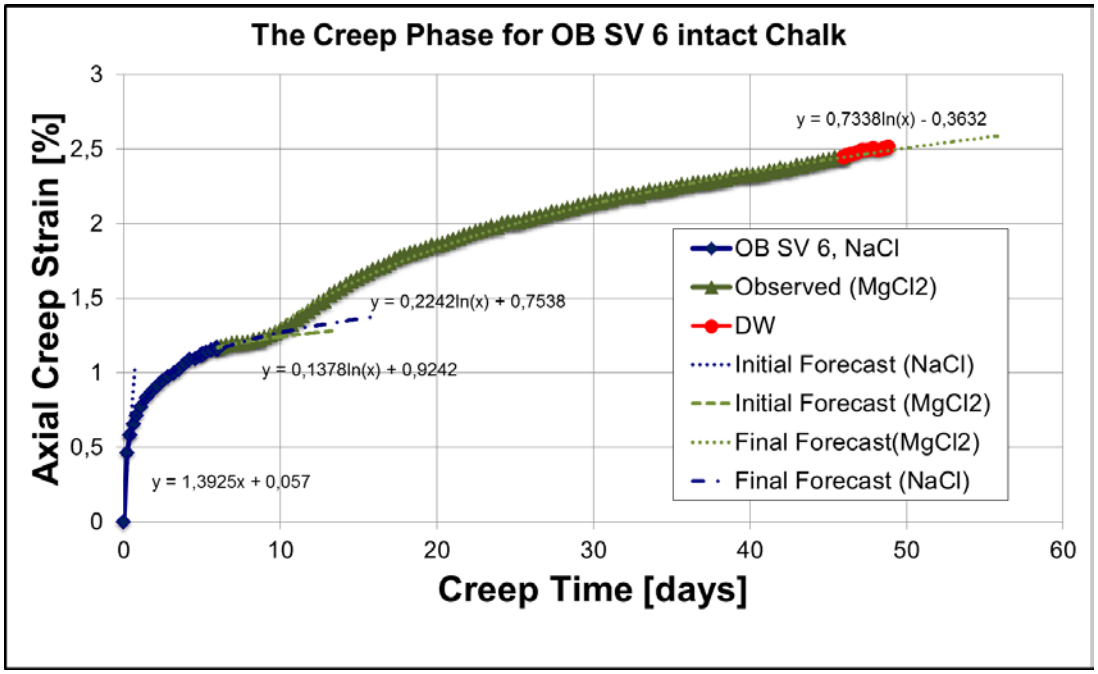

Figure 4.3: Axial Creep Strain [%] as a function of Creep Time [days] for OB SV 6 (Intact) was plotted. The core was flooded with 0.657 M NaCl for the first six days and the flooding fluid was switched to 0.219 M $MgCl_2$ for another 40 days. Unlike SSW, introduction of 0.219 M $MgCl_2$ did not trigger an immediate mechanical response. It took about three days for the core to show an accelerated creep after the brine change.

4.1.2 Chemical Analyses (Intact Cores)

The ion interaction between the chalk samples and the brine flooded was analyzed using Dionex ICS-3000 Ion Chromatography System. The evolution of ion concentration as function of water sampling time was plotted for all five of the core samples. In this section, the chemical analysis results for the intact cores will be presented.

Chemical Analysis; Intact Core OB SV 9 (SSW)

Fig. 4.4 shows the original and produced ion concentrations for Na^+ and Cl^- ions as a function of time. The ion concentrations in the effluent for both Na^+ and Cl^- did not deviate from the original ion concentrations (0.657 M NaCl), rather the values oscillate around the original values. Once the brine was changed to SSW, the ion concentrations in the effluent reduced from 0.657 to 0.525 M for Cl^- ion and from 0.657 to 0.45 M for Na^+ ion. However, the ion concentrations in the effluent were in

line with the original ion concentrations of both Na^+ and Cl^- in the SSW. Therefore, this infers neither Na^+ nor Cl^- had reacted chemically with the chalk core sample.

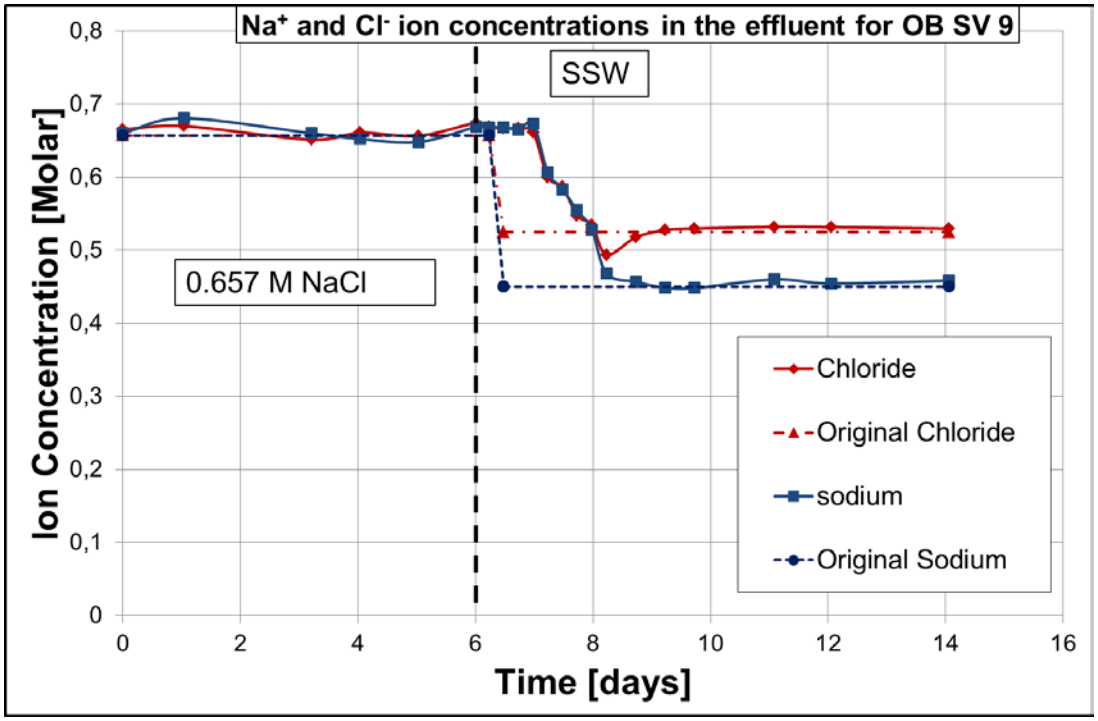

Figure 4.4: Na^+ and Cl^- Ion Concentration [M] as a function of water sampling time [days] for OB SV 9 (Intact).It is clearly seen that the ion concentrations of both Na+ and Cl- ions are more or less the same as their ion concentrations in the original 0.657 M NaCl and SSW.

In addition, the ion concentrations of magnesium (Mg^{2+}), calcium (Ca^{2+}) and sulfate (SO_4^{2-}) ions in the effluent and their original ion concentrations in the flooding brines were plotted as a function of water sampling time as shown on Fig. 4.5. During the first six days of sampling time, none of the ions were observed were observed in the effluent, except an average production of 0.00319M Ca^+ ions. This is expected since the core was only flooded with flooded with 0.657 M NaCl. The production of 0.00319M Ca^+ ions could be the result of dissolution process as the chalk surface reacted with the brine. Although the core was flooded with SSW starting day six, Mg^{2+} and SO_4^{2-} were not detected in the effluent until day 8. This could be because of the fact that the flooding fluid had to go through the entire rock matrix in intact cores as opposed to fractured cores. As depicted on Fig 4.5, starting day 8, SO_4^{2-}, Ca^{2+} and Mg^{2+} ions breakthrough and was detected in the effluent. It is interesting to observe that SO_4^{2-} and Ca^{2+} ions reached their highest concentrations

in the effluent just after their breakthrough time. After their high peaks, production of Ca^{2+} had steadily reduced and more and more of SO_4^{2-} ions were lost in the core. Further, high amount of Mg^{2+} ions were lost in the core. This means to some extent magnesium and sulfate were lost while calcium was gained. This clearly proved that there was some kind of chemical reaction between the ions in SSW and chalk sample. Three chemical reactions could occur; 1) substitution processes whereby magnesium ions replacing calcium ions, 3) dissolution of calcium carbonate and 2) precipitation of anhydrite ($CaSO_4$) when sulfate reacts with calcium. It seems like the amount of Mg^{2+} lost is equivalent to the amount of Ca^{2+} produced plus the amount of Ca^{2+} lost during the formation of anhydrite ($CaSO_4$). During the course of the experiment, it was not possible to flood in to the core after 20 days as the core was clogged. This clogging quite possibly was the result of anhydrite ($CaSO_4$) precipitation when sulfate reacts with the chalk.

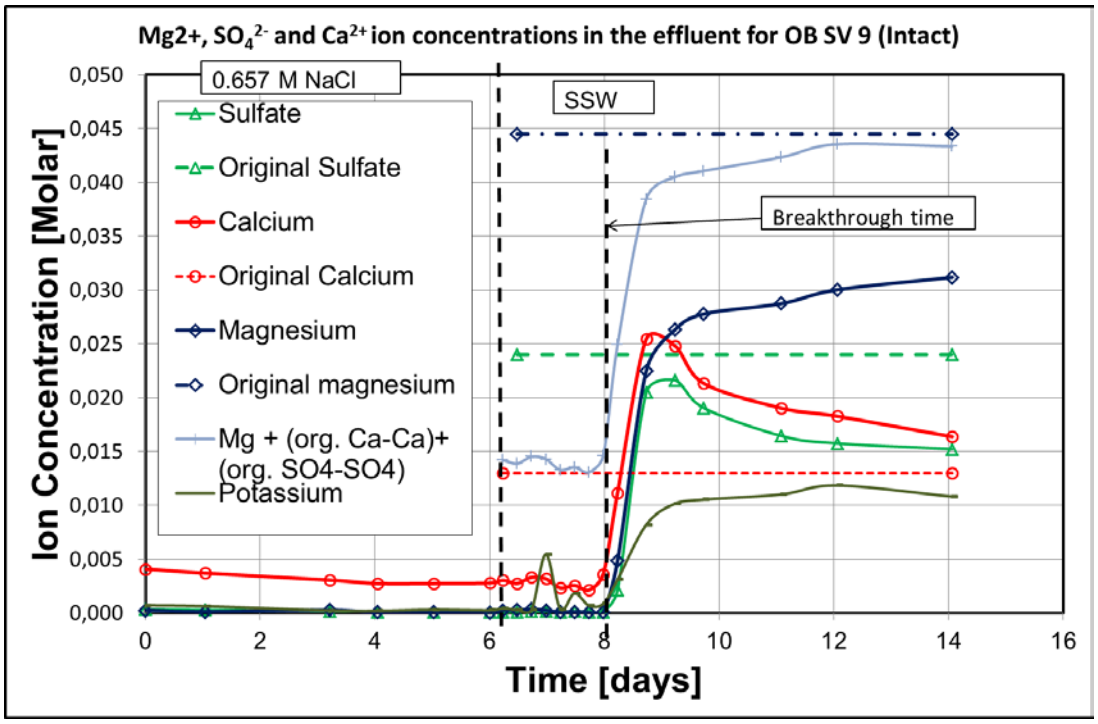

Figure 4.5: Mg^{2+}, Ca^{2+} and SO_4^{2-}, K^+ Ion Concentration [M] as a function of water sampling time [days] for OB SV 9 (Intact). High amount of magnesium ions were lost and production of calcium had attained its high peak just after the breakthrough time and then calcium production had reduced steadily. Relatively high amount of sulfate was observed after its breakthrough time and then more and more sulfate ions were lost in the core. Note also that it took about two days for the ions to breakthrough and seen in the effluent.

Chemical Analysis; Intact Core OB SV 6 (0.219 M $MgCl_2$)

Similarly, Fig. 4.6 shows the concentrations of Na^+ and Cl^- ions in the effluent as a function of time. The first and third samples show clear deviation from the originally flooded concentrations of Na^+ and Cl^- ions in 0.657 M NaCl brine. This could be the result of dilution during the chemical analysis. All water samples were diluted together at the same time except sample three. Sample three had to be diluted separately since there was an error during preparation for the chemical analysis. Otherwise, the concentrations of both Na+ and Cl^- seem to fluctuate around the original ion concentration. The moment the brine was changed to 0.219 M $MgCl_2$, Cl^- ion concentration reduced from an average value of 0.657 M to 0.438 M, and Na^+ ion concentration supposed to reach from 0.657 M to zero as expected. However, it seems that the concentration of Na^+ ion took about 32 days to reach to zero.

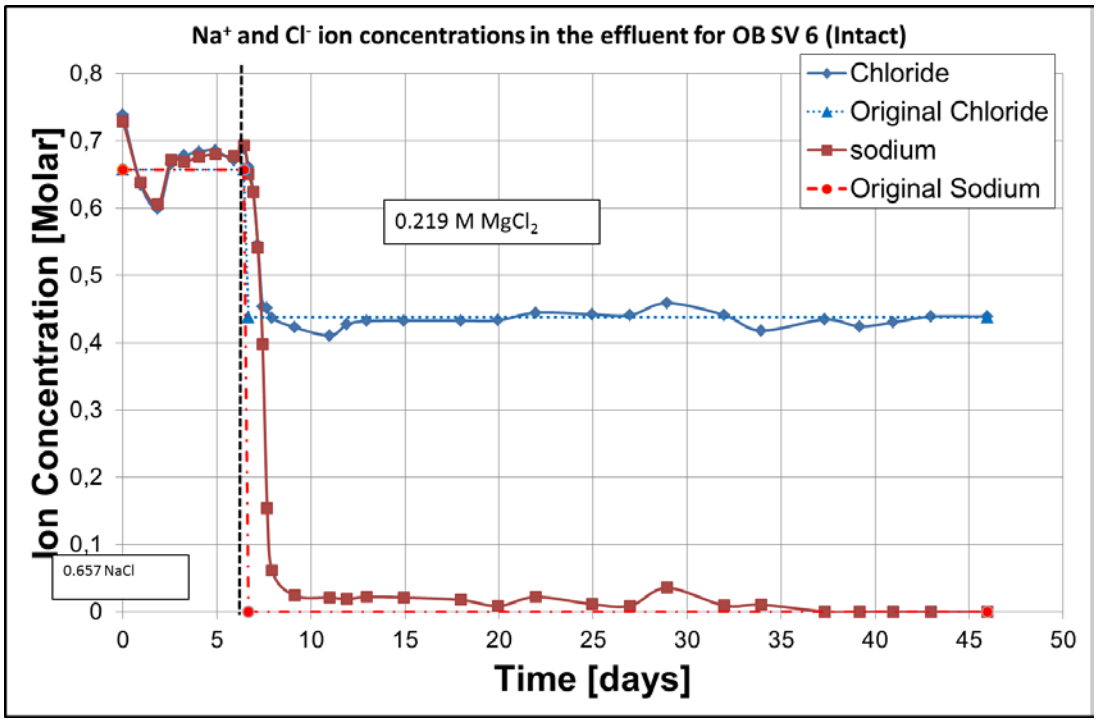

Figure 4.6: Na^+ and Cl^- Ion Concentration [M] as a function of water sampling time [days] for OB SV 6 (Intact).It is clearly seen that the ion concentrations of both Na+ and Cl- ions are more or less the same as their ion concentrations in the original 0.657 M NaCl and 0.219 M $MgCl_2$.

Further, Fig 4.7 shows the concentrations of magnesium (Mg^{2+}), calcium (Ca^{2+}) and combined (Mg^{2+} +Ca^{2+}) ions as a function of water sampling time. During $NaCl_2$, almost none of Mg^{2+} and Ca^{2+} ions were observed in the effluent. Once the brine was changed to $MgCl_2$ brine, high peak of Ca^{2+} was observed and then the production of Ca^{2+} had reduced steadily after the first peak. In the meantime, equivalent amount of Mg^{2+} ion was lost in the core. The combined (Mg^{2+} +Ca^{2+}) seem to be equal to the amount of Mg^{2+} ion flooded originally.

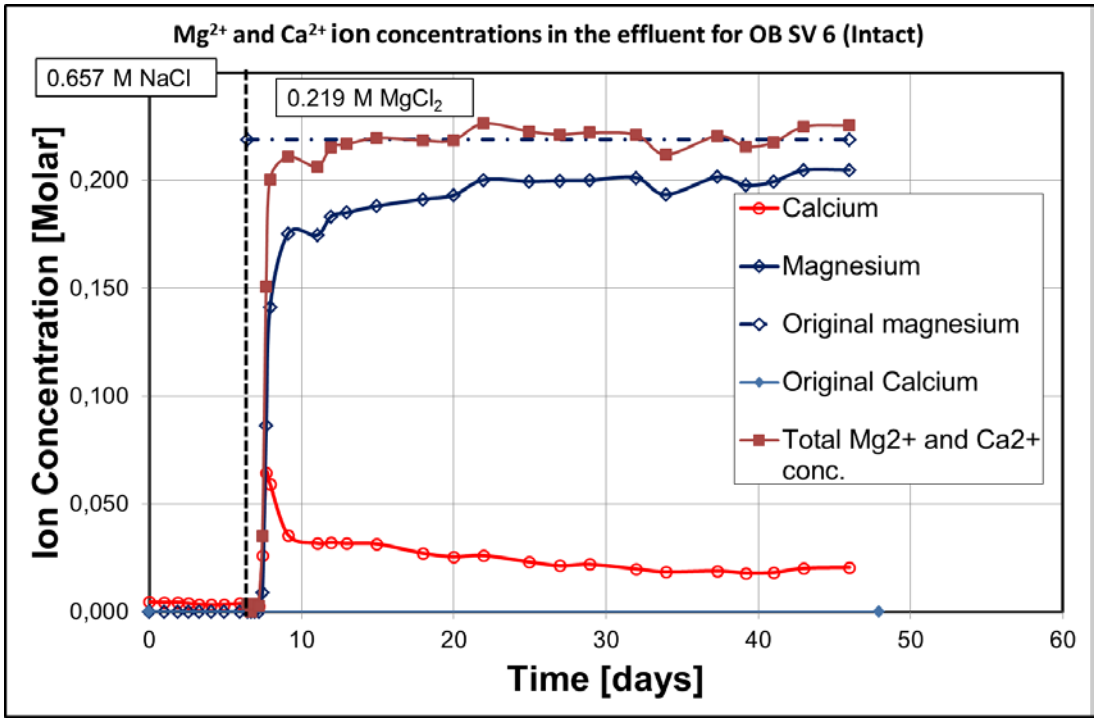

Figure 4.7: Mg^{2+} and Ca^{2-} Ion Concentration [M] as a function of water sampling time [days] for OB SV 6. Note that some amount of magnesium is lost in the core and an equivalent amount of calcium is produced. Also, high peak of calcium production was observed after breakthrough time, and then the production of calcium had steadily reduced. It is also important to note that it took about more than a day for the ions to breakthrough and be seen in the effluent.

4.1.3 Porosity Calculations (Intact Cores)

Please refer section 3.6 to understand how porosity calculations were made. The results found for the intact cores are summarized in Table 4.4. The porosity calculations results showed that there is a considerable amount of porosity reduction after the mechanical tests were performed. This is an expected result as it is evident

that the cores would undergo mechanical and chemical compaction during the mechanical testing. The porosity of OB SV 9 has reduced from 41.34% to 37.02 % and its density has reduced from 2.69g/cm^3 to 2.67g/cm^3, whereas the porosity of OB SV 6 has reduced from 40.81 % to 38.6% and its density has increased from 2.68g/cm^3 to 2.72g/cm^3. The change in density could be the result of mineral precipitation during the creep experiments. Also, the change in porosity was not only the result of mechanical compaction; rather it is the combination of mechanical compaction and chemical compaction that could result from mineral precipitation.

Table 4.4: Volume, mass, density and porosity data before and after the test for intact cores.

Core Sample	V_B [CC]		ε_v	M_s [g]		ρ[g/cc]		ϕ [%]			
	B	A		B	A	B	A	B		A	
								M	M+C	M	M+C
OB SV 9	80	75.4	0.0575	126.57	127.26	2.69	2.67	41.34	41.34	37.76	37.02
OB SV 6	79.8	75.6	0.052	126.65	126.28	2.68	2.72	40.81	40.81	37.55	38.6

Where B is before test, A is after test, M is mechanical and M+C is mechanical and chemical.

4.2 Fractured Chalk Samples (OB SV 4, OB SV 12 and OB SV 18)

4.2.1 Mechanical Test

Similar to the intact core samples the mechanical tests for fractured cores comprised of two distinct parts; the hydrostatic phase and the creep phase. During the hydrostatic phase, the core samples were loaded hydrostatically, beyond their yield point, until the confining pressure reaches approximately 12 MPa (This point was chosen to load the cores 2.5-3MPa beyond the yield point). During this phase all the samples were flooded with 0.657 M NaCl at the rate of 1 pore volume per day (PV/day). Following the hydrostatic phase the samples were left to creep under constant confining pressure of 12 MPa.

4.2.1.1 The Hydrostatic Phase (Fractured Cores)

Similarly, the mechanical strengths of the fractured cores during the hydrostatic loading are shown in Fig. 4.8. Table 4.5 summarizes the results during the hydrostatic loading for the fractured chalk core samples.

It was observed that OB SV 12, with porosity of 41.34% and length of 68.54, has shown total axial strain of 1.071%, yield strength of 9 MPa and K-value of 0.622 GPa. The other two cores, OB SV 4 and OB SV 18, showed similar mechanical properties although the latter one has higher porosity. Note that the excellent repeatability of the hydrostatic tests. The results found showed very similar, if not the same, yield strength and K-values as presented in Table 4.5.

Table 4.5: Mechanical test results during hydrostatic loading for the fractured cores. The fractured cores have shown amazing similarities in yield strength and K-values. This indicates that hydrostatic tests have excellent repeatability.

Core Sample	Porosity [%]	Length [mm]	Yield Strength [MPa]	K-Value [GPa]	Total axial Strain [%]
OB SV 4	40.49	68.81	9.4	0.73	0.8145
OB SV 12	41.34	68.54	9.0	0.622	1.071
OB SV 18	41.18	68.28	9.4	0.73	0.857

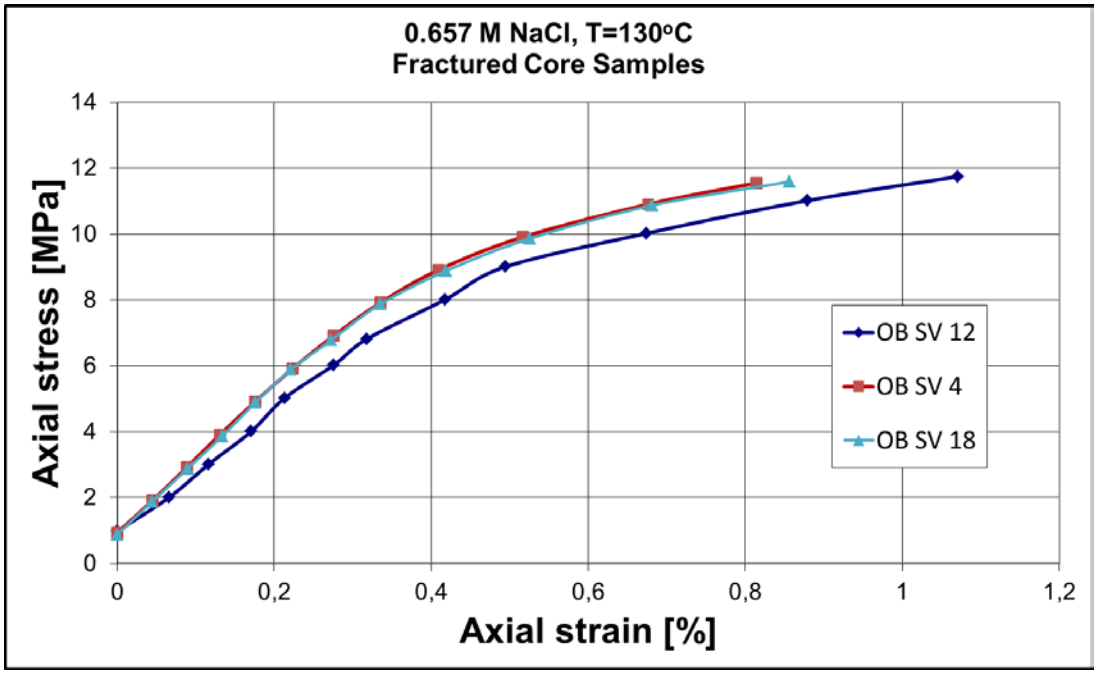

Figure 4.8: Axial Stress [MPa] Plotted as a function of axial strain [%] for the fractured cores (OB SV 4, OB SV 12 and OB SV 18). The results show that the yield strength and the K-values are very similar (the yield curves are more or less overlapping). However, intact chalk OB SV 12 showed a deviation from the other two cores and that might be because of its high porosity.

4.2.1.2 Creep Phase (Fractured Cores)

The creep phase of the experiment was started the moment the confining pressure reached 12MPa (which is at the end of the hydrostatic loading phase). During this period constant confining pressure of 12MPa was kept until the end of the test and type of fluid was switched from NaCl to other desired fluids. The total axial strain that was recorded during the hydrostatic loading was not part of the strain that was found during the creep phase. To show the deformation of the core samples under constant stress, axial strain after the hydrostatic loading versus time was plotted in all the experiments. The creep phase results for the intact cores are summarized in Table 4.6. The results presented in Table 4.6 are described in more detail in the following sections.

Table 4.6: Summary of Flooding brine, total axial creep strain and creep strain rates for fractured cores. Fractured core OB SV 4 was flooded with 0.657 M NaCl brine for six days and followed by 0.219 M $MgCl_2$ brine for about 58 days. Fractured core OB SV 12 was flooded with 0.657 M NaCl brine for the first six days and followed by SSW for about 53 days. Fractured core OB SV 18 was flooded with 0.657 M NaCl brine for the entire test period of 24 days

Core Sample	Flooding Fluid	Flooding Periods [days]		Volume Flooded [ml]	Total Axial Creep Strain [%]	Initial Strain rate, [%/decade]	Final Strain rate, [%/decade]	
		Start	Stop					
OB SV 4	NaCl	0	5.74	181.84	1.25	---	1.76	
	$MgCl_2$	5.74	64	1845.68	2.60	0.58	5.98	
	DW	64	68	---	2.64	---	---	
OB SV 12	NaCl	0	6	198.72	1.59	---	2.18	
	SSW	6	59	1755.36	3.326	3.31	8.15	6.56
	DW	59	65.6	---	3.39	---	----	
OB SV 18	NaCl	0	24	752	1.67	---	1.75	

The Creep Phase; Fractured Core OB SV 4 (0.219M $MgCl_2$)

For the first six days of the creep phase, OB SV 4 was flooded with 0.657 M NaCl and it was switched to 0.219 M $MgCl_2$ as shown in Table 4.6. Further, Fig. 4.9 shows how flooding of $MgCl_2$, after NaCl flooding stopped, changed the trend of the creep curve. During the first six days, the creep strain rate followed logarithmic trend and the observed value was 1.76 %/decade. After six days, total axial creep strain of 1.25% was observed. It would have followed the same trend, if NaCl brine was kept as the flooding fluid as it was forecasted (see Fig.4.9). However, the flooding fluid was switched to $MgCl_2$ after the sixth day. For approximately four days after the switch, $MgCl_2$ brine had not contributed more on the creep than what was observed during the final days of NaCl brine flooding. During this time only about 0.58 %/decade creep strain rate was observed. But it was after these four days,

the effect of $MgCl_2$ on the creep started to show up. Final Strain rate of 5.98 %/decade was observed starting day 10 until the end of the experiment. The final strain rate has increased more than 10 times compared to what was observed during the initial four days of $MgCl_2$ flooding. After approximately 64 days, total axial creep strain of 2.6% was observed. Then the core was cleaned with distilled water for about four days. After cleaning the core, total axial strain of 2.64% was observed. Based on observation, the accelerated creep phase is very much dependent upon time and the response of the core was only seen after four days since the $MgCl_2$ brine was introduced.

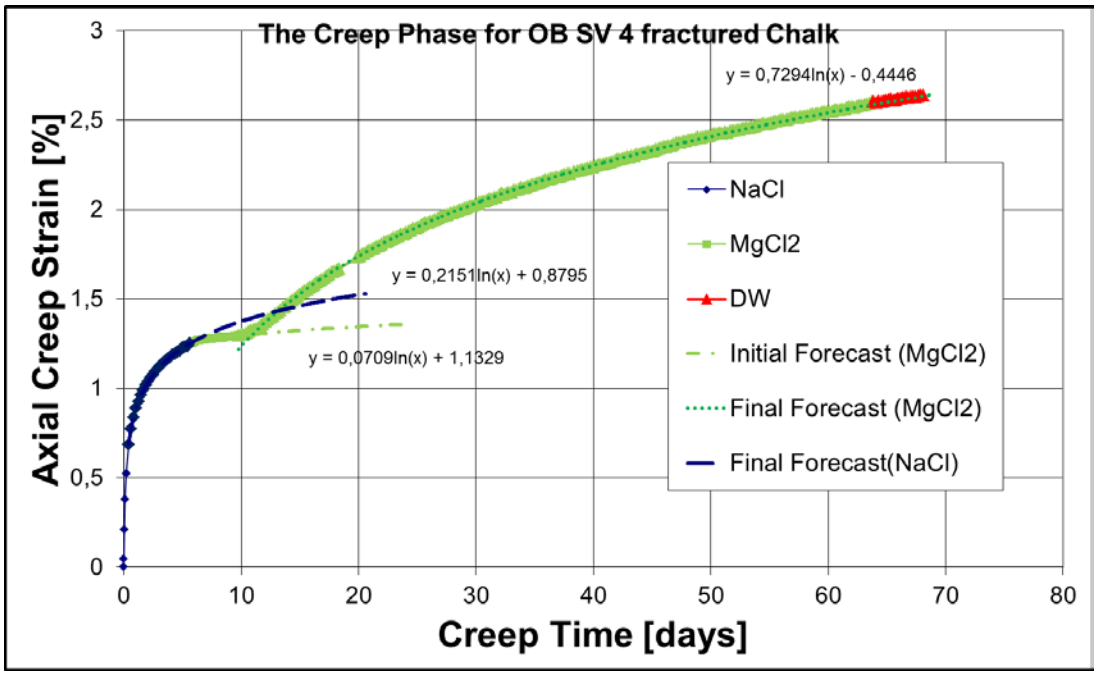

Figure 4.9: Axial Creep Strain [%] as a function of Creep Time [days] for OB SV 4. Unlike SSW, introduction of 0.219 M $MgCl_2$ did not trigger an immediate mechanical response. It took about four days for the core to show an accelerated creep after the brine change. Note that the response time for the fractured core (OB SV 4) was longer than the intact core (OB SV 6)

The Creep Phase; Fractured Core OB SV 12 (SSW)

For the first six days of the creep phase, OB SV 12 was flooded with 0.657 M NaCl and it was switched to synthetic sea water (SSW) as shown in Table 4.6. Unlike $MgCl_2$, the effect of SSW on the creep strain had been seen immediately after the

NaCl flooding was switched to SSW flooding as show in Fig. 4.10. This suggested that SSW flooding was not very much time dependent as the response of the creep curve was immediate.

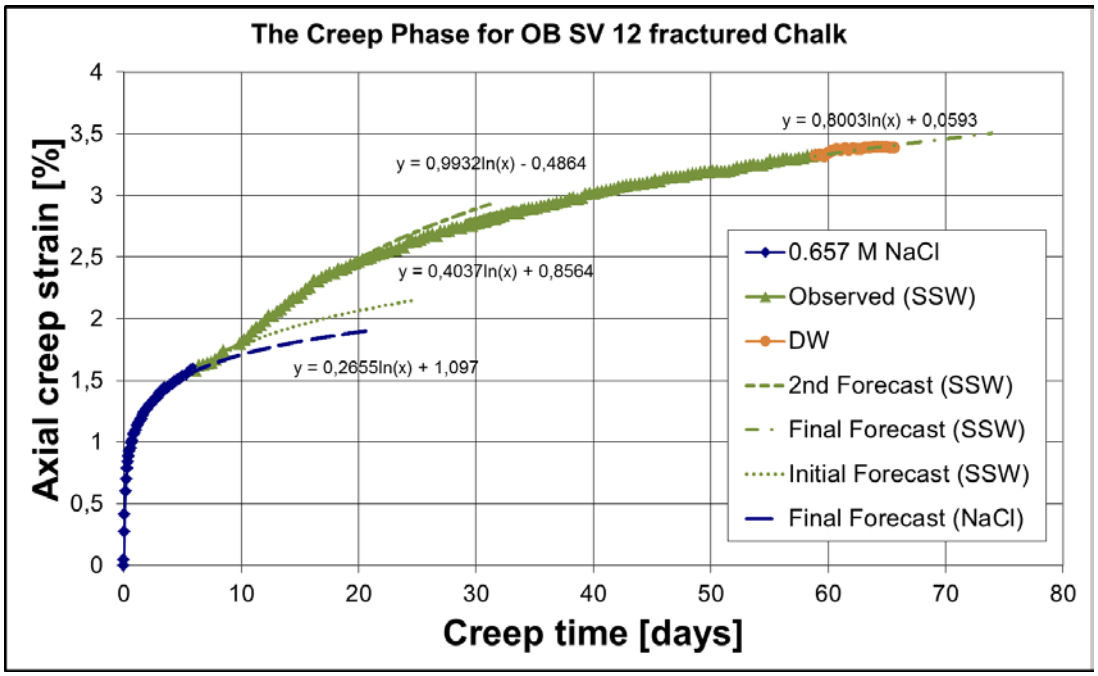

Figure 4.10: Axial Creep Strain [%] as a function of Creep Time [days] for OB SV 12 fractured core was plotted. The core was flooded with 0.657 M NaCl for the first six days and the flooding fluid was switched to SSW for another 53 days. Immediately after brine change, it was observed mechanical response of the core.

As depicted on Fig. 4.10, during NaCl flooding, the creep strain followed logarithmic trend and the creep strain rate was 2.18 %/decade. After six days, 1.59% total axial creep strain was observed. If NaCl had been used for the entire test, the creep strain rate would have been only 2.18%/decade as it was forecasted using logarithmic trend. However, the NaCl brine had been switched to SSW to observe what effect it might have on the creep. It turned out, after the switch the creep strain rate had increased immediately from 2.18 to 3.31 %/decade, which is 1.52 times increase. The creep strain rate even increased more from 3.31 to 8.15%/decade after four days since the brine change. Further, the creep strain rate reduced from 8.15 to 6.56 %/decade after 10 days since the switch and continued with the same rate for the rest of the experimental period. After approximately 59 days, total axial creep

strain of 3.33% was observed. After cleaning the core with distilled water for about seven days, total axial strain of 3.39% was observed.

The Creep Phase; Fractured Core OB SV 18 (0.657M NaCl)

Unlike the other cores, OB SV 18 was flooded with 0.657 M NaCl for the entire time. The creep curve followed a logarithmic trend and the creep strain rate was 1.75 %/decade. Since only 0.657 M NaCl was used as the flooding fluid for the entire test, no change on the strain rate was observed for the entire test as shown on Fig 4.11. After 24 days of testing, final axial creep strain of 1.67% was observed.

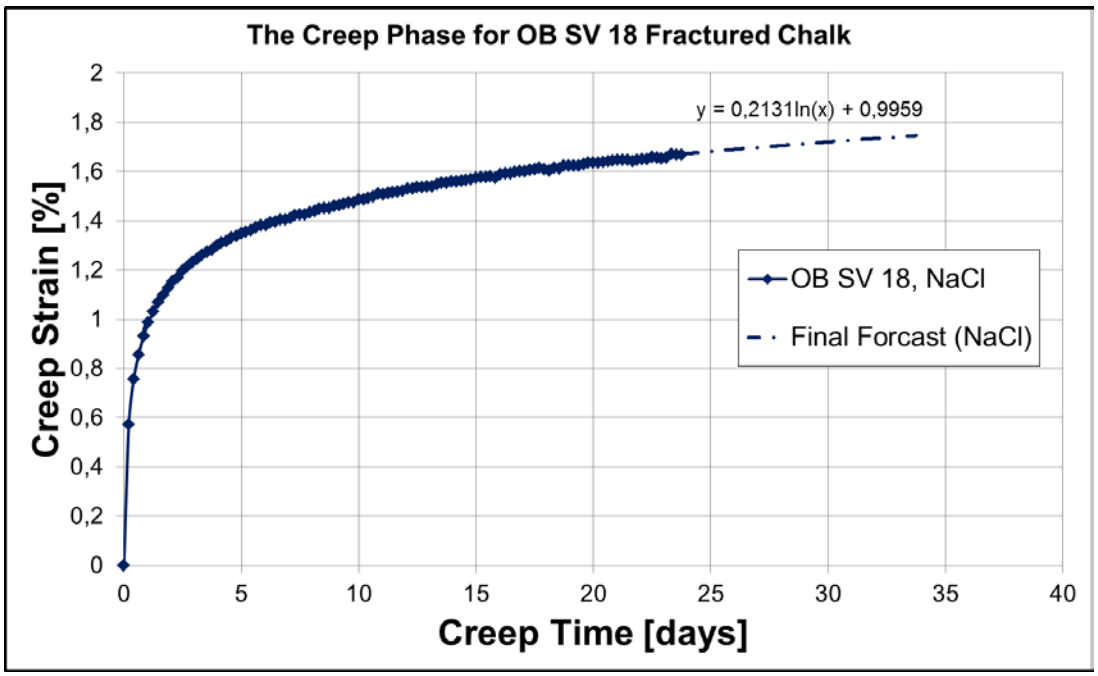

Figure 4.11: Axial Creep Strain [%] as a function of Creep Time [days] for OB SV 18 fractured core was plotted. It was flooded with 0.657 M NaCl brine for the entire test period of 24 days. Unlike $MgCl_2$ and SSW brines, no change of creep strain rate had been observed during 0.657 M NaCl flooding.

4.2.2 Chemical Analyses (Fractured Cores)

In this section, the ion concentrations from the chemical analysis as a function of water sampling time was plotted for the fractured chalk core samples.

Chemical Analysis; Fractured Core OB SV 4

Fig. 4.12 shows ion concentrations of Na^+ and Cl^- ions in the effluent as a function of time. Approximately the same amount of Na^+ and Cl^- ions that were originally injected were produced. That means the produced ion concentration for both Na^+ and Cl^- did not deviate from the original ion concentrations (0.657 M NaCl), rather the values oscillate around the original values. This clearly suggests that neither Na^+ nor Cl^- did interact with the chalk surface. When the flooding fluid switched to 0.219 M $MgCl_2$, the production of Na^+ ions reduced to zero as there was no any Na^+ ions present in $MgCl_2$ brine. In addition, the production of Cl^- had reduced from 0.657 M to 0.438 M when the flooding fluid was switched to $MgCl_2$ brine as expected.

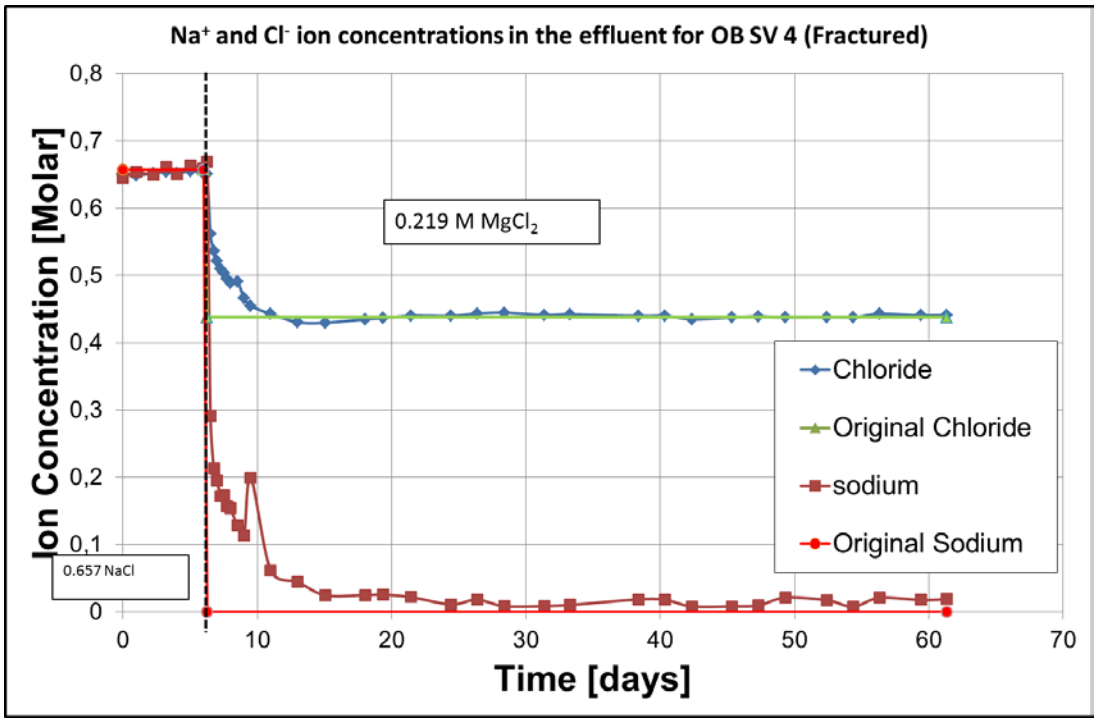

Figure 4.12: Na^+ and Cl^- Ion Concentration [M] as a function of water sampling time [days] for OB SV 4 (Fractured).It is clearly seen that the ion concentrations of both Na+ and Cl- ions are more or less the same as their ion concentrations in the original 0.657 M NaCl and 0.219 M $MgCl_2$.

Further, Mg^{2+} and Ca^{2-} ion concentrations in the effluent as a function of water sampling time [days] was plotted as shown on Fig. 4.13. During $NaCl_2$, almost no amount of Mg^{2+} and Ca^{2-} were detected in the sampled brine. The moment the brine was switched to $MgCl_2$, both Mg^{2+} and Ca^{2-} started to be seen in the effluent. However, the produced Mg^{2+} ion concentration was less than what had been injected. On the other hand, higher amount of Ca^{2-} ions had been produced compared to what was originally injected and the combined concentrations of both Mg^{2+} and Ca^{2+}ions were plotted to check if it is as much as the original Mg^{2+} ion concentration. It turned out the combined (Mg^{2+} + Ca^{2-}) ion concentration was approximately the same as the original Mg^{2+} ion concentration. This clearly shows that as much as the loss of Mg^{2+} ions, there was equivalent amount of Ca^{2-} ions production. However, this didn't mean that the loss of magnesium and production of calcium was merely due to substitution process.

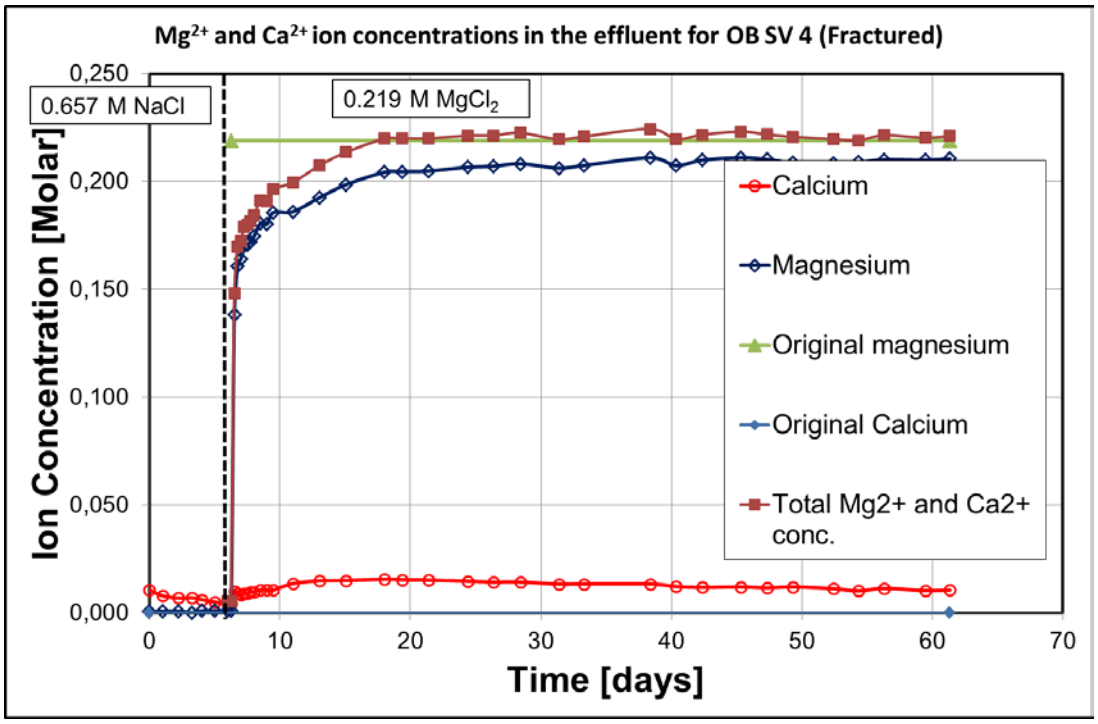

Figure 4.13: Mg^{2+} and Ca^{2-} Ion Concentration [M] as a function of water sampling time [days] for fractured core OB SV 4. Note that some amount of magnesium lost in the core and an equivalent amount of calcium is produced. It is very interesting to see that, unlike the intact chalk, no high peak calcium was observed after breakthrough time. The amount of loss of Mg^{2+} and production of Ca^{2-} is lower as compared to intact core OB SV 6 flooded with same brine (0.219 M $MgCl_2$). It is also important to note that the breakthrough time is very short, if not immediate, as compared to the intact chalk (OB SV 6).

Chemical Analysis; Fractured Core OB SV 12 (SSW)

As it has been done for the other chalk samples, Na^+ and Cl^- ion concentrations in the effluent as a function of water sampling time was plotted as shown on Fig 4.14. Similar trend was seen as the other cores, which is the ion concentrations of both Na^+ and Cl^- ions in the effluent seem to oscillate around the original concentrations. However, there are some inconsistencies with some of the peaks. The first peak of Na^+ seems to be higher than what was originally injected during NaCl brine flooding (0.657 M NaCl). Further, after the brine was changed to SSW, at day 14 both Na^+ and Cl^- ion concentrations are higher than what was originally injected (See Fig. 4.14). Also, these consistencies seen with $Ca^{2+,}$ Mg^{2+} and SO_4^{2-} showing high peaks at day 14 (see Fig. 4.15). These inconsistencies could be the result of human errors made during water sampling or the result of dilution during sample preparation for chemical analysis.

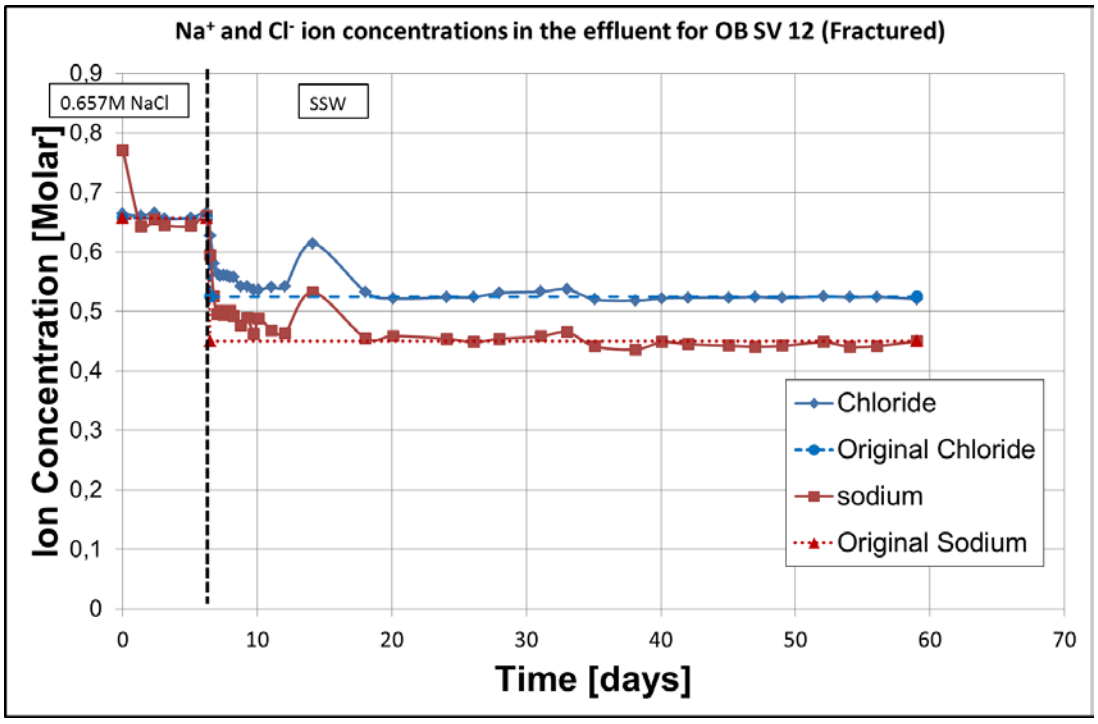

Figure 4.14: Na^+ and Cl^- Ion Concentration [M] as a function of water sampling time [days] for OB SV 12 (Fractured).It is clearly seen that the ion concentrations of both Na+ and Cl- ions are more or less the same as their ion concentrations in the original 0.657 M NaCl and SSW. However, higher peaks of Na+ and Cl- were seen at day 14. The same high peaks were observed for Mg^{2+}, Ca^{2+} and SO_4^{2-} at the same time (see Fig. 4.15). This could be the result of human errors during water sampling or dilution.

Further, the Mg^{2+}, Ca^{2+}, K^{+} and SO_4^{2-} ion concentrations in the sampled water is shown on Fig. 15. When the flooding brine was changed to SSW, the production of Mg^{2+}, Ca^{2+}, K^{+} and SO_4^{2-} ions had started. As depicted on Fig. 4.15, some of the injected Mg^{2+} and SO_4^{2-} ions lost in the core, higher amount of Ca^{2+} ions were produced compared to originally injected, and equivalent amount of K^{+} produced compared to what was originally injected. Note that at day 20 higher amount of SO_4^{2-} (0.06 M) and Ca^{2+} (0.0365 M) ions were produced compared to the original SO_4^{2-} (0.024 M) and Ca^{2+} (0.013) ion concentrations, respectively. Most importantly, the amount of SO_4^{2-} lost in this fractured core flooded with SSW is very small as compared to the intact core OB SV 9 flooded with SSW.

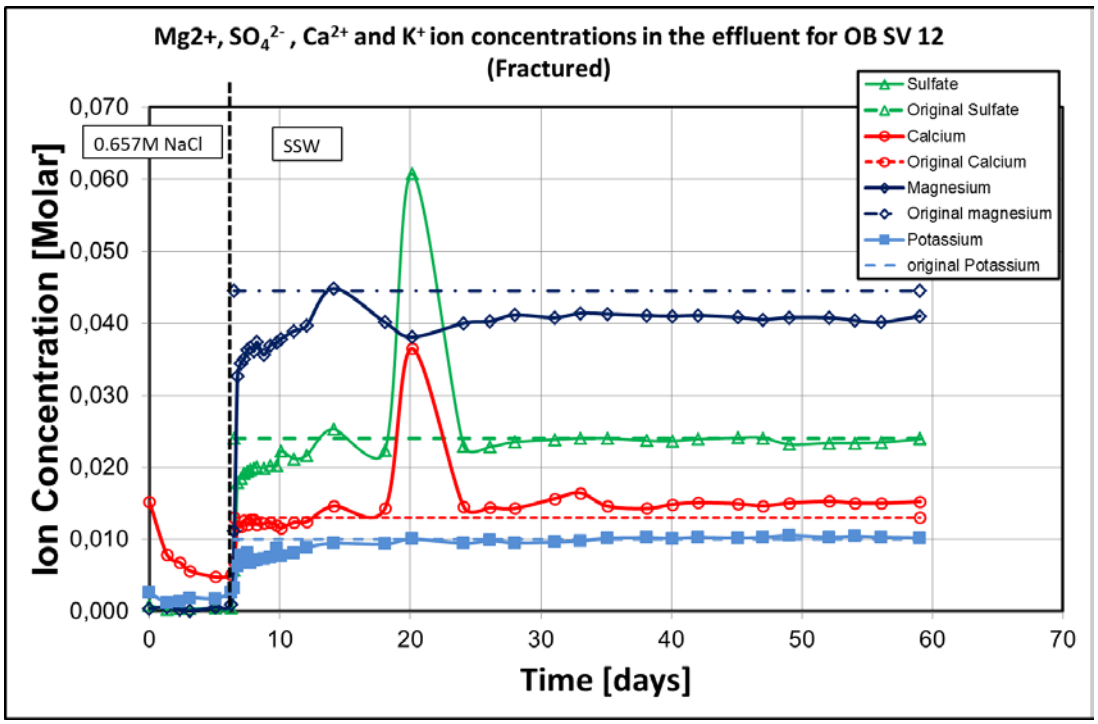

Figure 4.15: Mg^{2+}, Ca^{2+} and SO_4^{2-}, K^{+} Ion Concentration [M] as a function of water sampling time [days] for OB SV 12 (Fractured). Considerable amount of magnesium ions were lost. No high peaks of calcium and sulfate was observed, after breakthrough time, as opposed to the intact chalk OB SV 9 flooded with the same brine (SSW). The amount of SO_4^{2-} lost in this core is considerably low as compared to the intact chalk OB SV 9. In addition, the loss of Mg^{2+} and production of Ca^{2+} was lower than what was observed for the intact chalk OB SV 9. Note also that the breakthrough time for this core is very fast as compared to the intact core OB SV 9.

4.2.3 Porosity Calculations (Fractured cores)

Please refer section 3.6 to understand how porosity calculations were made. The results found for the fractured cores are summarized in Table 4.7. Similar to the intact cores, the porosity calculations results showed that there is a considerable amount of porosity reduction after the mechanical tests were performed. This is an expected result as it is evident that the cores would undergo mechanical and chemical compaction during the mechanical testing. The porosity of OB SV has reduced from 40.49% to 37.95 % and its density has increased from 2.69g/cm^3 to 2.73g/cm^3, whereas the porosity of OB SV 12 has reduced from 41.34 % to 37.15 and its density has increased from 2.7g/cm^3 to 2.74g/cm^3. The change in density could be the result of mineral precipitation during the creep experiments. Also, the change in porosity was not only the result of mechanical compaction; rather it is the combination of mechanical compaction and chemical compaction that could result from mineral precipitation.

Table 4.7: Volume, mass, density and porosity data before and after the test for fractured cores.

Core Sample	V_B [CC]		ε_v	M_s [g]		ρ[g/cc]		ϕ [%]			
	B	A		B	A	B	A	B		A	
								M	M+C	M	M+C
OB SV 4	78.38	73	0.0688	125.23	123.96	2.69	2.73	40.49	40.49	38.08	37.95
OB SV 12	78	71.5	0.0832	123.56	123.18	2.7	2.74	41.34	41.34	36.02	37.15

Where B is before test, A is after test, M is mechanical and M+C is mechanical and chemical.

5 DISCUSSIONS

All the results acquired from creep experiments agree with the notion that the aqueous chemistry of the flooding fluid plays an important role on the water weakening effects on tested chalk samples. The tested cores showed different degrees of mechanical response depending on the type of flooding fluid as well as whether the cores are intact or fractured. The presence of fractures resulted in less chemical deformation compared to intact cores as the travel path of the chemical ions injected eased by the fractures inside the core. However, it is worth to note that the presence of fractures inside the cores had not totally hindered the water weakening effects of Mg^{2+} and SO_4^{2-} on the tested cores. It seemed as though there was considerable amount of chemical interaction between the fluids inside the fractures and the walls of the fractures. This implied that the fluids not only flow through the fractures but also diffuse into the core matrix. The effect of effective stress was observed in one of the cores; a reduction in effective stress resulted in less amount of creep strain. The SEM-EDS analysis also revealed the formation of new magnesium-bearing minerals.

5.1 Similarities in Mechanical Strength during hydrostatic loading

It comes as no surprise that the tested Mons core samples had shown incredible similarities in terms of their yield strength and K-values (see Table 5.1, Figs. 5.1 and 5.2). The similarities observed were mainly due to the fact that all the tested cores were extracted from the same outcrop chalk as well as they were drilled from the same block. Since all the cores were drilled and extracted from the same outcrop block, the effect of anisotropy on the mechanical properties of the cores is minimal. This results exactly corresponds to the results found in Korsnes et al. (2008), which is “mechanical properties are only directly comparable when the chalk samples are collected and drilled in the same direction from the same block of chalk.” It is worth noting that regardless of the fractures introduced the tested cores had shown very similar mechanical strengths. This infers that the presence of fractures did not significantly influence the mechanical properties of the cores during hydrostatic loading. However, the minor differences seen, in mechanical properties, had to be

because of the porosity variations between the cores and the 2mm hole artificial fracture introduced in three of the cores (OB SV 4, OB SV 12 and OB SV 18). The most important conclusion from the hydrostatic tests is the excellent repeatability of these tests and the results withdrawn can be trusted.

Table 5.1: Summary of Mechanical results during hydrostatic loading. It is evident that the results have shown incredible similarities regardless of porosity variations and the introduction of 2mm hole fracture in three of the cores (OB SV 4, OB SV 12 and OB SV 18)

Core Sample	Porosity [%]	Length [mm]	Yield Strength [MPa]	K-Value [GPa]	Total axial Strain	Description
OB SV 6	40.81	70	9.6	0.68	0.795	Intact
OB SV 9	41.34	70.1	9.4	0.67	0.904	
OB SV 12	41.34	68.54	9.0	0.622	1.071	Fractured
OB SV 18	41.18	68.28	9.4	0.73	0.857	
OB SV 4	40.49	68.81	9.4	0.73	0.8145	

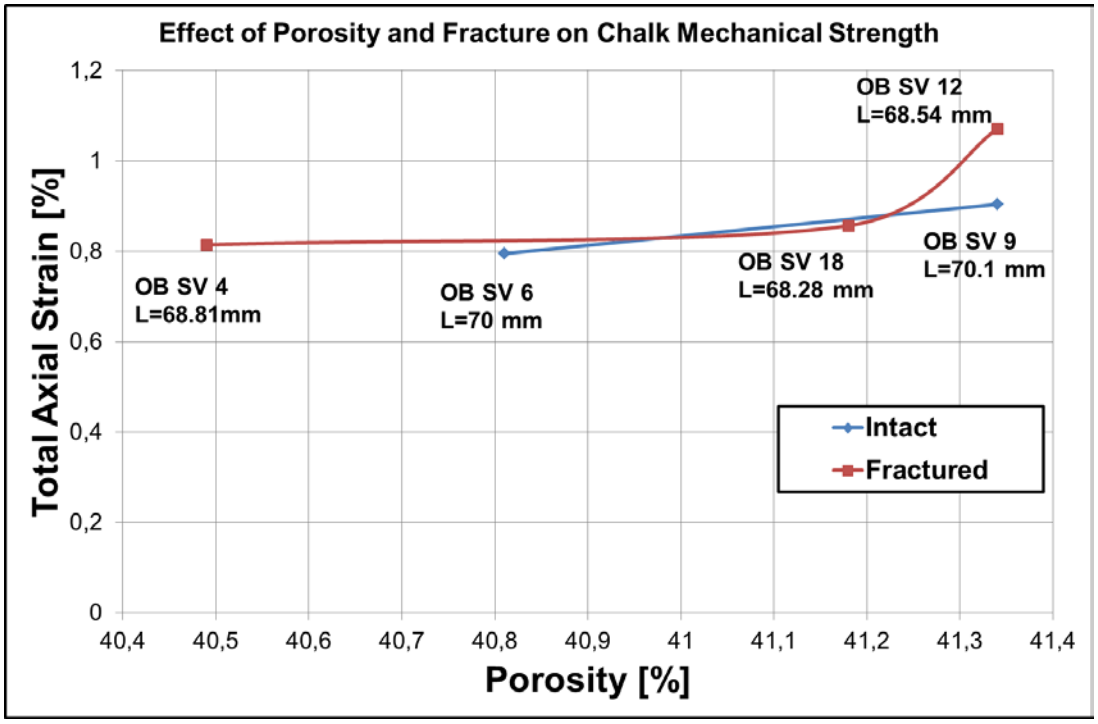

Figure 5.1: Total axial strain [%] is plotted as a function of porosity [%] for both intact and fractured cores. The differences in axial strains between the fractured and intact cores during hydrostatic loading are minor.

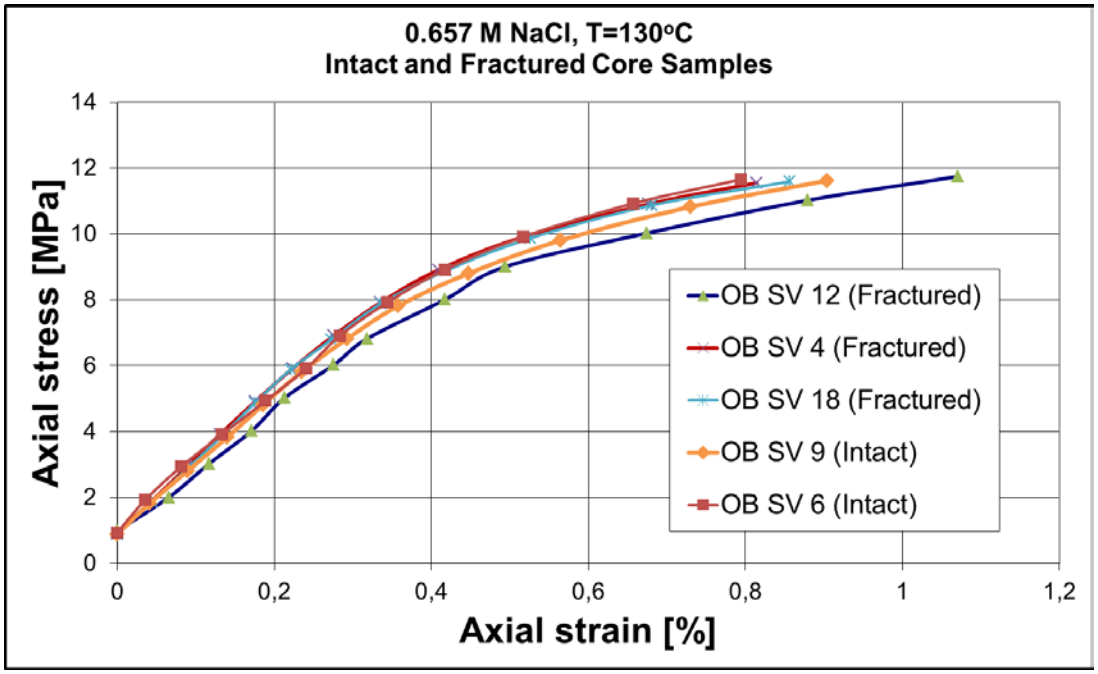

Figure 5.2: Axial Stress [MPa] Plotted as a function of axial strain [%] for both intact and fractured cores. The results show that the yield strength and the K-values are very similar. The yield curves are more or less overlapping although there is a minor difference that resulted from porosity variations as well as fractures.

5.2 Creep Phase Analyses

Comparison of creep strain results for the tested cores have led us to believe that the types of fluids injected and the presence of fractures inside cores impact the chemical deformation. These observations were further backed by the chemical analyses, porosity calculations and SEM image results. Here, the effects of effective stresses, flooding fluid content, presence of fractures inside the tested cores and the analysis from SEM-EDS will be mainly discussed (creep strain rates were taken as the criteria to compare rather than creep strain values).

5.2.1 Effect of Effective Stress on Creep Strain

The impact of effective stress on creep strain was seen when the intact chalk sample (OB SV 9) was flooded with SSW. During the course of the experiment the core was clogged as a result of the precipitation of anhydrite ($CaSO_4$). The $CaSO_4$ could be the result of chalk surface ($CaCO_3$) interaction with sulfate. The formation of the $CaSO_4$ resulted in high pore pressure inside the core. The normal pore pressure that was set during the experiment was about 70 bars. However, when the core was clogged, the pore pressure had increased from 70 to maximum of 90 bars since the differential pressure between the inlet and the outlet of the core was increased. This means the effective stress that acts on the core had reduced as the pore pressure increased due to high differential pressure (see Fig. 5.3). The reduction in effective stress resulted in less amount of creep strain as shown on Fig 5.3 between day 15 and 18. To reduce the pore pressure, the bypass valve was opened to stop flooding in to the core. This helped the pore pressure to stabilize back to its normal value of 70 bars. Then the effective stress had increased as the pore pressure reduced. Consequently, the creep strain increased after day 18 as shown on Fig. 5.3.

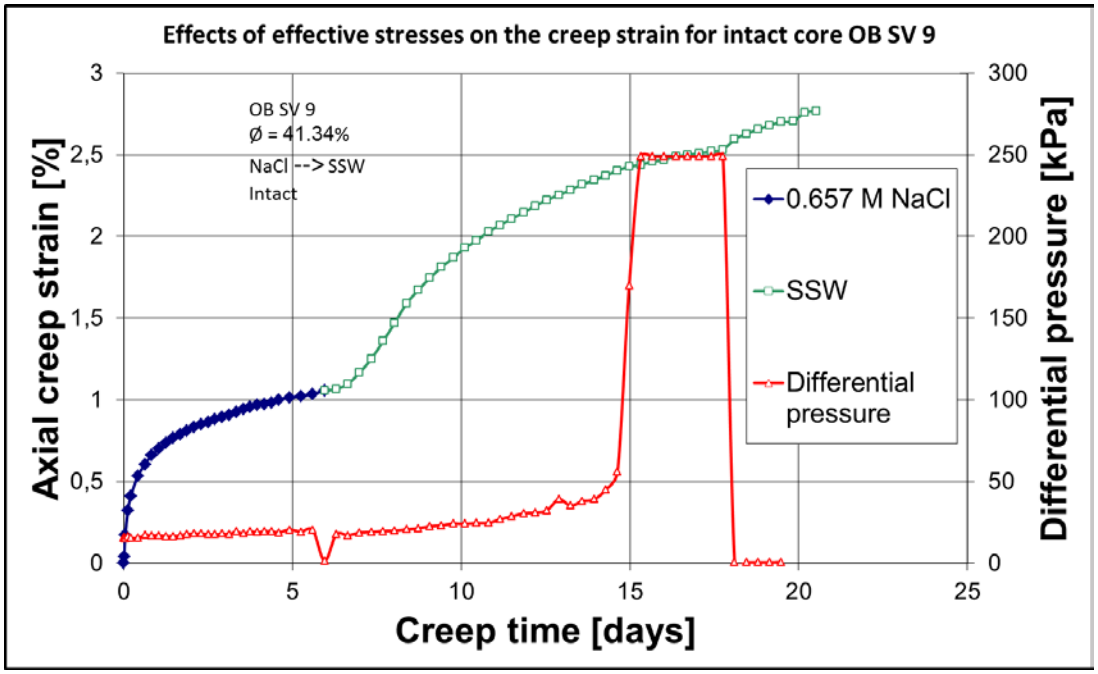

Figure 5.3: Axial creep strain [%] and Differential Pressure [kPa] were plotted as a function of creep time [days] for intact core OB SV 9 during SSW flooding. The formation of $CaSO_4$ caused the core to be clogged and as a result the differential pressure increased (the jump is seen on the figure). This ultimately increased the pore pressure; as a result the effective stress had reduced. Therefore, the chemical deformation of the core had reduced.

5.2.2 Effects of Flooding Fluid Content with respect to Creep

The aqueous chemistry of the flooding fluid seemed to be the reason for the various mechanical responses of the tested cores. This trends has been reported previously by Korsnes et al. (2006), Madland et al. (2011), and Megawati et al. (2012). Madland et al. (2011) performed mechanical tests on Liege cores with 0.219 M $MgCl_2$ as the flooding fluid and argued that sulfate was not needed to have a significant amount of deformation and that the deformation was comparable with deformation caused by SSW. To check their hypothesis, mechanical tests were performed on intact and fractured Mons chalks with 0.657 M NaCl, 0.219 M MgCl2 and SSW as the flooding brines. The comparisons were made in such a way that the effects of the injected brines were seen on the creep curves; not the effects of the fractures. To achieve this, the three fractured cores flooded with different brines were compared and then the two intact cores flooded with different brines were compared. On Fig 5.4, the axial creep strains of the fractured cores (OB SV 18, OB SV 4 and OB SV 12) as a function of creep time were plotted to show the

comparison made for the fractured chalk samples flooded with 0.657M NaCl, 0.219M $MgCl_2$ and SSW, respectively. As shown on Fig. 5.4, the core flooded with 0.657 M NaCl (OB SV 18) for the entire time showed a steady final strain rate of 1.75%/decade and this was an expected observation as the Na^+ and Cl^- ions are chemically inert to the chalk surface. The core that was flooded with 0.219 M $MgCl_2$ showed a surprising behavior; it seemed as though the creep strain rate had stopped, if not, reduced from what had been seen before the brine was changed. However, after 4-5 days of testing the creep started to accelerate from 0.58 to 5.98 %/decade, which is an increase by more than a factor of 10. This kind of behavior was reported in Madland et al. (2011) and other previous experiments that were performed on cores with $MgCl_2$ as the flooding brine. It is interesting to see that the flattening of the creep curve was not observed with the core that was flooded with SSW; rather the mechanical response was immediately observed when the flooding fluid was switched from NaCl to SSW. However, in Haddadi (2013) experimental work, Kansas chalk flooded with SSW, the mechanical response was not seen immediately after the brine was switched from formation water to SSW. This could be because of the strength of the chalk used in Haddadi (2013) work (Kansas chalk); Kansas chalk is much stronger and compact compared to Mons chalk. In addition, Haddadi (2013) used NaCl brine but higher ion concentration in the first six days of the experiment as opposed to 0.657 M NaCl used in this study. As shown on Fig 5.4, the core flooded with SSW has shown higher creep strain than the core flooded with 0.219 M $MgCl_2$. This was because of the effect of SO_4^{2-} on creep strain at the start of brine switch. Interestingly, however, after 50-60 days the final creep strain rate observed for the core flooded with SSW was 6.56%/decade whereas for the core flooded with 0.219 M $MgCl_2$ was 5.98%/decade. This suggested that if we had been able to flood the same core with SSW and 0.219 M $MgCl_2$ alternatively, the resulting chemical deformation, as SSW flooding fluid, would have been just only 1.1 times more than what we would have observed with $MgCl_2$ as the flooding brine. Thus, the comparison between the two fractured cores OB SV 4 (0.219M MgCl2) and OB SV 12 (SSW) showed that small differences in creep strain rates in the long run.

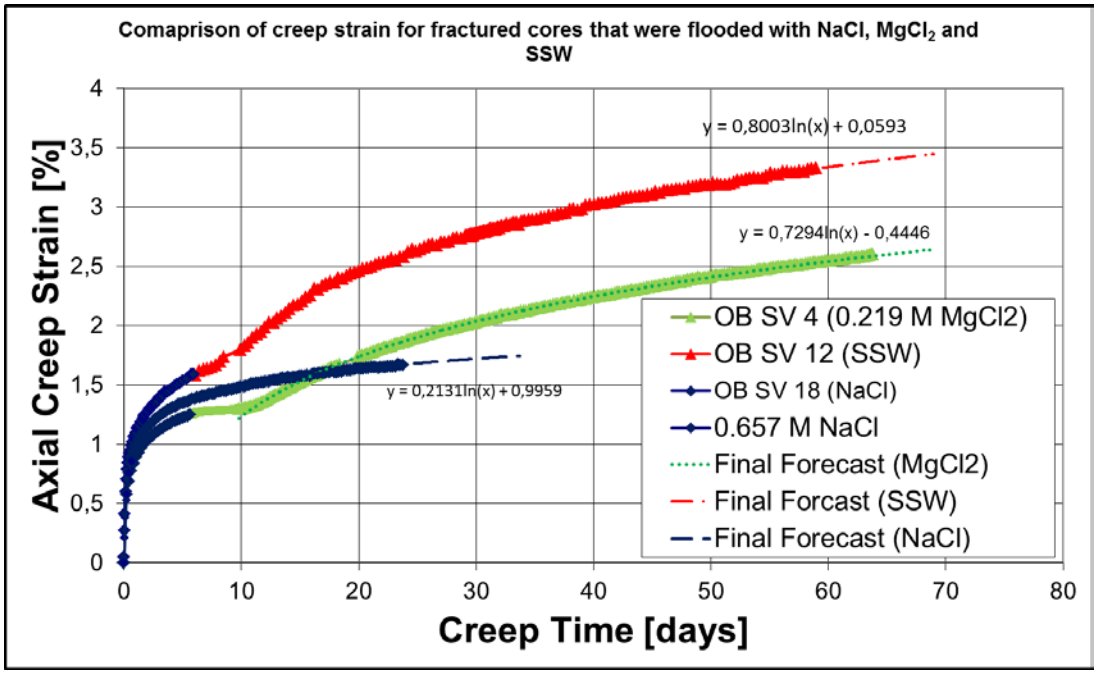

Figure 5.4: Axial creep strain [%] Plotted as a function of creep time [day] for the fractured cores (OB SV 4, OB SV 12 and OB SV 18) to compare the mechanical response of the tested cores for various flooding fluids. Fractured core OB SV 18 flooded with 0.219M NaCl had shown final strain rate of 1.75%/decade. Fractured core OB SV 4 flooded with 0.219M $MgCl_2$ had shown final strain rate of 5.98%/decade. Fractured core OB SV 12 flooded SSW had shown final strain rate of 6.56%/decade. The two cores flooded with SSW and $MgCl_2$ showed small differences in creep strain after 50-60 days.

Further, comparison of the intact chalks, OB SV 9 and OB SV 6, flooded with SSW and 0.219 M $MgCl_2$, respectively, was made by plotting the creep strains as a function of creep time (see Fig. 5.5). The core flooded with SSW (OB SV 9) had shown higher creep strain rates than the core flooded with 0.219 M $MgCl_2$ (OB SV 6). Quantitatively, the final creep strain rate observed for the intact core flooded with SSW was 9.28%/decade whereas for the intact core flooded with 0.219M $MgCl_2$ was 6%/decade; a reduction by a factor of 1.54. This suggested that the chemical deformation observed for intact cores flooded with SSW and 0.219 M $MgCl_2$ was not comparable and that the core flooded with SSW would creep 1.5 times more than the core flooded with 0.219 M $MgCl_2$.

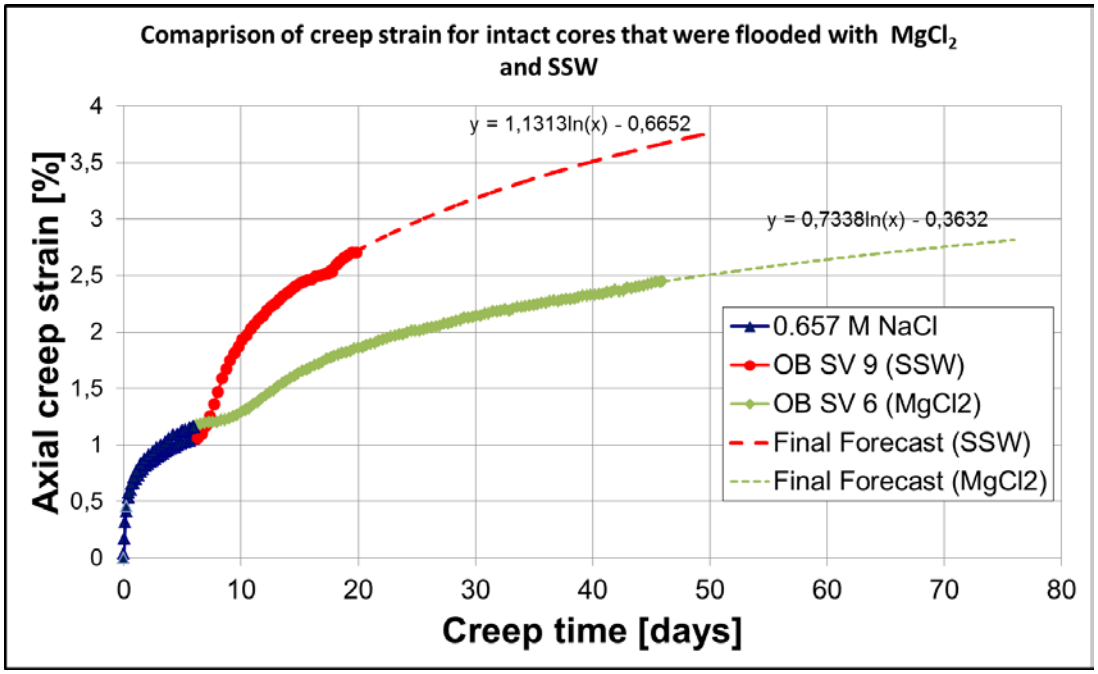

Figure 5.5: Axial creep strain [%] Plotted as a function of creep time [day] for the intact cores (OB SV 9 and OB SV 6) to compare the mechanical response of the tested cores for various flooding fluids. It is clearly seen from the plot that intact core OB SV 9 flooded with SSW had shown superior creep strain rates (9.28%/decade) than intact core OB SV 6 flooded with 0.219M $MgCl_2$ (6%/decade).

5.2.3 The Role of Magnesium (Mg^{2+}) and sulfate (SO_4^{2-}) ions with respect to creep

Having seen the various mechanical responses with respect to flooding brine, we further performed chemical analyses to understand the role of the different ions on the chemical deformation. The role of Mg^{2+} is seen clearly on Figs. 5.6 and 5.7. We can clearly see that significant amount of magnesium is lost in the core and additional amount of calcium is produced. Comparison of Figs. 5.6 and 5.7, in terms of the amount of Mg^{2+} ions lost and Ca^{2+} ions gained, shows that the amount Mg^{2+} ions lost and Ca^{2+} gained were higher for the intact core OB SV 6 than for the fractured core OB SV 4. Note also that the breakthrough time of Mg^{2+} and Ca^{2+} for the intact core was longer as compared to the fractured core. However; both Figs. 5.6 and 5.7 show that the combined calcium production and loss of magnesium concentrations are approximately equal to the original concentration of magnesium in 0.219 M $MgCl_2$ injected. This simple observation might lead to a conclusion that substitution process is the only mechanism. Madland et al. (2011), however, have pursued further and performed calculations to quantify the amount of magnesium

lost inside the core. Their result showed the amount of magnesium lost was too high just to be by simple substitution process. Therefore, there had to be something going on other than substitution of calcium by magnesium. The extra loss of magnesium could be justified by the formation of other newly formed minerals. For the cores flooded with 0.219 M $MgCl_2$, the formation of dolomite ($CaMg(CO_3)_2$) or huntite ($CaMg_3(CO_3)_4$) is highly likely. Therefore, we further made density analysis on the tested cores after the mechanical experiments were performed and compared the new densities with the original densities of the cores. It was interesting to observe that both cores tested with 0.219 $MgCl_2$ (OB SV 4 and OB SV 6) showed higher densities than their original densities. OB SV 4 (fractured) showed an increase in density from 2.685g/cm^3 to 2.738g/cm^3 whereas OB SV 6 (intact) showed an increase in density from 2.681g/cm^3 to 2.719g/cm^3. The change in densities had to be related with the newly formed minerals inside the core when magnesium reacted with chalk grains ($CaCO_3$). Simple observation might lead to indicate dolomite is the newly formed mineral as its density (2.84g/cm^3) is higher than the density of calcite (2.8-2.7g/cm^3).

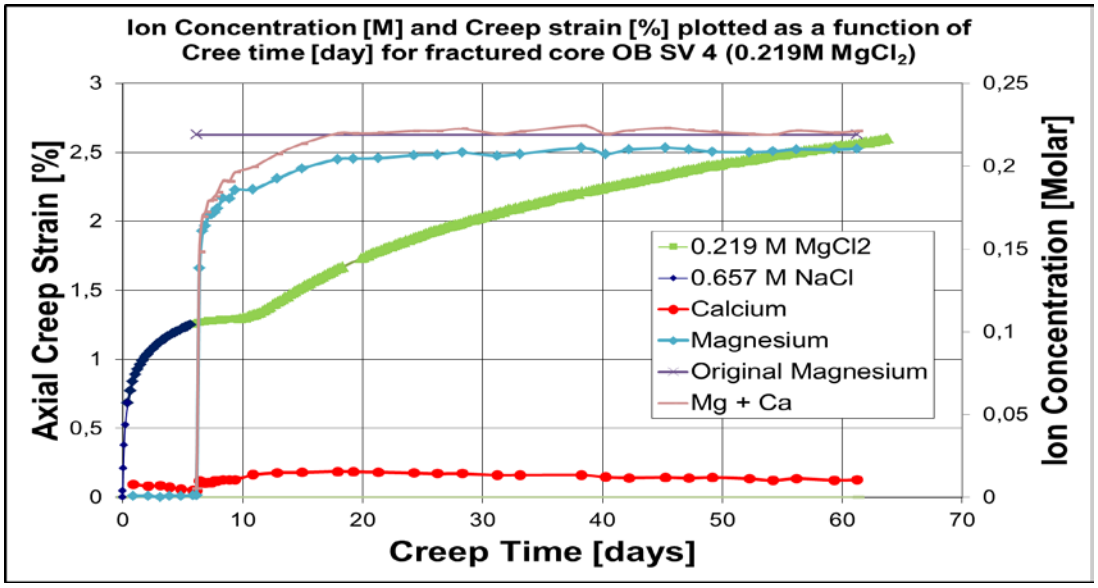

Figure 5.6: Axial creep strain [%] and Ion Concentration [Molar] Plotted as a function of creep time [day] for OB SV 4 (Fractured) flooded with 0.219M $MgCl_2$. Although the core is fractured, considerable amount of Mg^{2+} lost in the core and Ca^{2+} was gained. The breakthrough time of Mg^{2+} and Ca^{2+} is very fast as opposed to the intact core OB SV 6 (see fig 5.7). No high peak of Ca^{2+} as opposed to intact core.

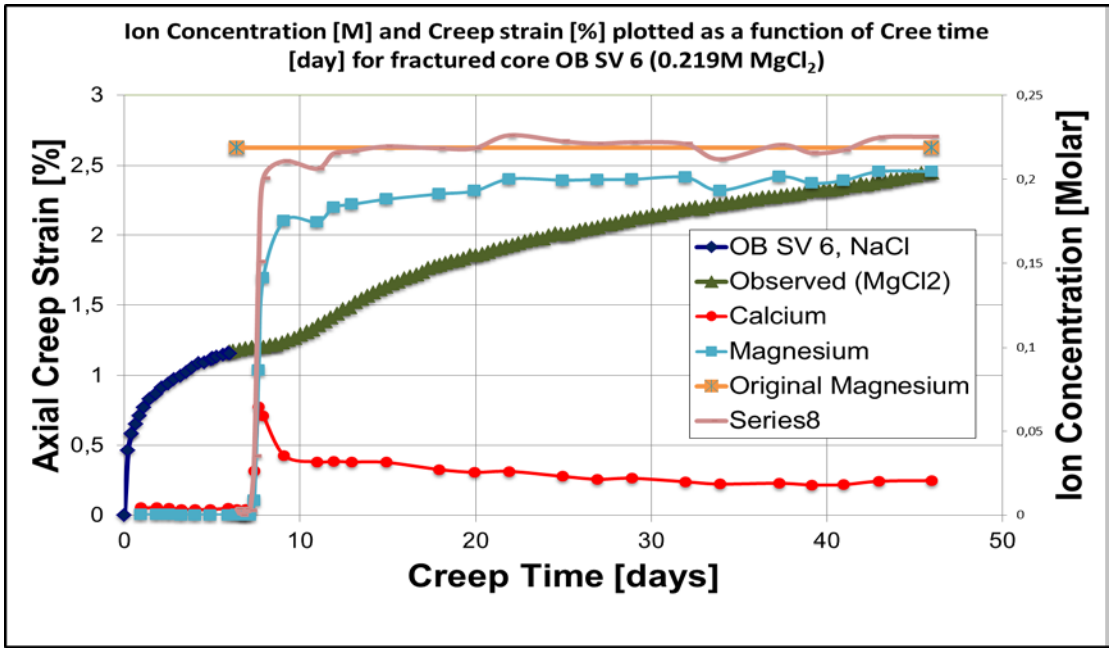

Figure 5.7: Axial creep strain [%] and Ion Concentration [Molar] Plotted as a function of creep time [day] for OB SV 6 (Intact) flooded with 0.219M $MgCl_2$. Higher amount of Mg^{2+} lost in the core and Ca^{2+} was gained relative to fractured core OB SV 4. The breakthrough time is longer as opposed to the fractured core OB SV 4 (see fig 5.6). High peak of Ca^{2+} production after breakthrough as opposed to fractured core was observed.

Further, we examine the role of sulfate on mechanical response of the core samples tested. In previous reports it was shown that the absence of sulfate would not really hinder the response of the creep curve as long as enough amount of magnesium ions are present in the flooding brine. However, Fig 5.8 (plotted to show the axial creep strain and ion concentrations of sulfate, magnesium and calcium as a function of creep time for intact core OB SV 9 flooded with SSW) confirms that there was significant amount of sulfate and magnesium lost in the core and additional amount of calcium was produced. Moreover, the tested cores flooded with SSW showed higher deformation than cores flooded with 0.219 M $MgCl_2$. Therefore, there had to be something that sulfate ions are doing to the cores. Megawati et al. (2012) reported that sulfate adsorbed to calcite surface and creates a negative surface charge. This negative surface charge could give rise to a total disjoining pressure which can be the reason for alteration of the mechanical properties of the chalk. In addition, precipitation of newly formed mineral cannot be ruled out. When the sulfate reacts with chalk grains there is possibility of forming new minerals like anhydrite ($CaSO_4$) and gypsum ($CaSO4.2(H_2O)$). The density analysis performed on cores

flooded with SSW showed an alteration of densities from the original densities of the cores. OB SV 9 (intact) showed a decrease in density from 2.697g/cm^3 to 2.68g/cm^3 whereas OB SV 12 (fractured) showed an increase in density from 2.7g/cm^3 to 2.74g/cm^3. These density variations had to be the result of newly formed minerals

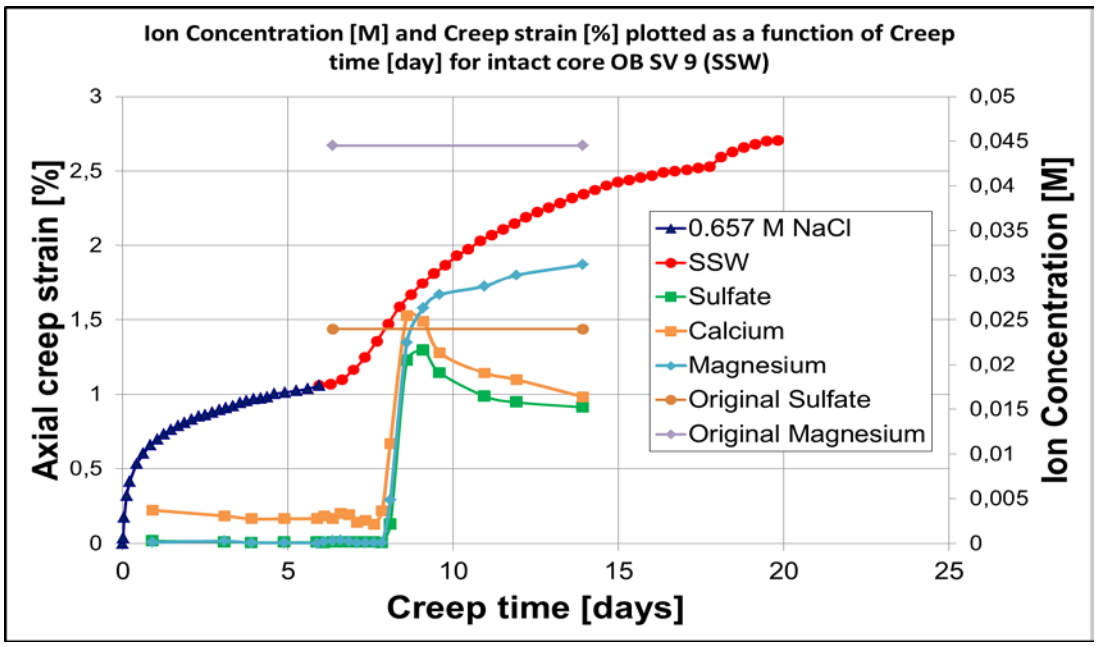

Figure 5.8: Axial creep strain [%] and Ion Concentration [Molar] Plotted as a function of creep time [day] for OB SV 9 (intact) flooded with SSW. Considerable amount of Mg^{2+} and SO_4^{2-} lost in the core and Ca^{2+} was gained. The breakthrough time of Mg^{2+}, Ca^{2+} and SO_4^{2-} is longer as opposed to the fractured core OB SV 12 (see fig 5.9). High peak of SO_4^{2-} and Ca^{2+} production after breakthrough time as opposed to fractured core OB SV 12 was observed.

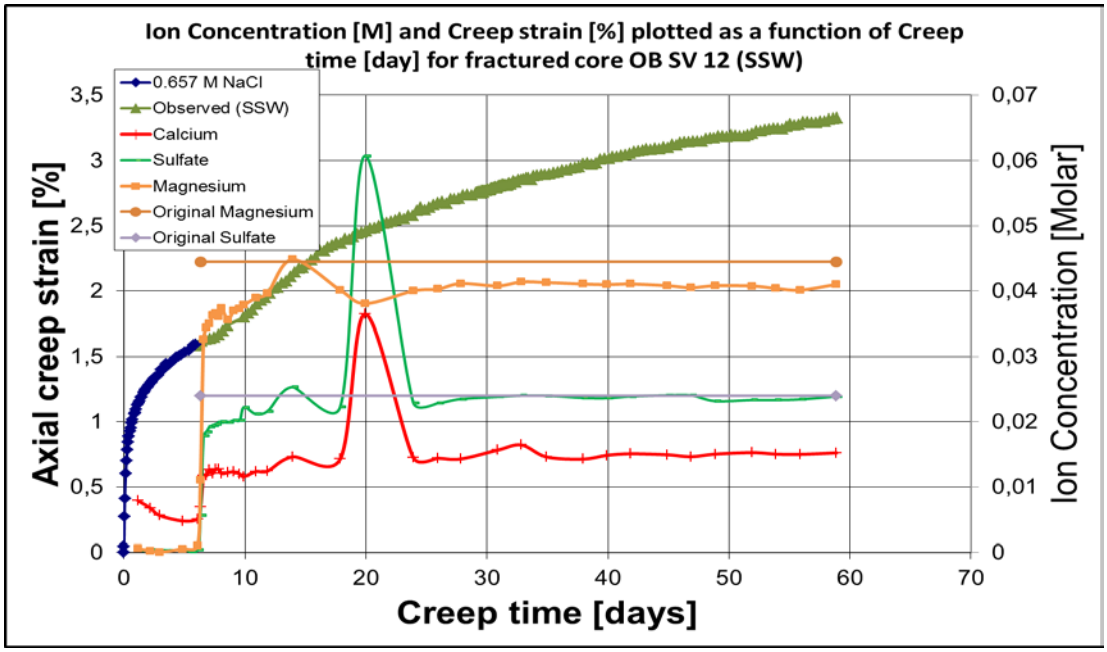

Figure 5.9: Axial creep strain [%] and Ion Concentration [Molar] Plotted as a function of creep time [day] for OB SV 12 (Fractured) flooded with SSW. Considerable amount of Mg^{2+} was lost in the core and Ca^{2+} was gained. However, the loss of the amount of SO_4^{2-} is minor. The breakthrough time of Mg^{2+}, Ca^{2+} and SO_4^{2-} is very fast as opposed to the intact core OB SV 9 (see fig 5.8).

5.2.4 The Effect of Fractures with respect to Creep

The magnitudes of creep strains seem to be affected by the presence of fractures in the tested chalk sample. This is best seen on Fig 5.10, which shows the comparison of two Mons Chalk samples that were flooded with synthetic sea water (SSW). The major difference between the two cores was the 2 mm hole (fracture) that was artificially introduced in one of the cores during testing. As depicted on Fig 5.10, although the fractured chalk sample creeps with higher creep strain rate than the intact chalk sample during 0.657 M NaCl flooding; this was not the case when the flooding fluid was switched to SSW. The moment the flooding fluid was changed to SSW, the intact chalk sample accelerated with higher creep strain rate than the fractured chalk sample. From day six to nine, the creep strain rate for the intact chalk was 16.51%/decade and for the fractured chalk was 3.31%/decade. This means within those three days the intact chalk creep strain had accelerated 4.99 times the creep strain of the fractured chalk, which we can clearly see on Fig 5.10. After day nine, the intact chalk creep strain curve overtook the creep strain curve of the fractured chalk. Further, the creep strain rates for both cores were predicted using

logarithmic trend to analyze the fate of both cores in terms of creep. The prediction showed that the intact chalk would creep more, with a rate of 9.28%/decade, as compared to the fractured chalk (6.56%/decade). The reason for this phenomenon could be explained by the difference in fluid transport mechanisms between intact and fractured chalk. The compactness of intact chalk would force the flooding fluid to travel through the pore spaces. This creates great opportunity for chemical interaction between chalk grains and the flooding fluid. However, on the other hand, the presence of fractures in chalks would allow the flooding fluid to take the easy way out, which is the flooding fluid to travel through the fractures as they pose less resistance to fluid transport. Thus, the chalk grains far from the fracture wall would not have the exposure to the flooding brine. As a result, the chalk grains far from the fracture wall would remain relatively strong. However, it is very important to note that the presence of fractures had not totally hindered the chemical interactions between the fluid and chalk surface. This is evidently seen in the chemical analyses of all fractured cores that Mg^{2+} and SO_4^{2-} were lost and Ca^{2+} was gained; this only happened if there was an interaction between fluids and chalk surface. Therefore, the injected fluid not only flow through the fracture, but also diffuses into the matrix

Having established the hypothesis that the retention time to flood through intact core was longer than the fractured core, chemical analyses were performed and the ion break through time in the effluent was analyzed for both cores. For the intact core flooded with SSW (OB SV 9), the breakthrough time for divalent ions (Mg^{2+}, SO_4^{2-} and Ca^{2+}) was approximately two days (see Fig. 5.8). For the fractured core flooded with SSW (OB SV 12), the breakthrough time for divalent ions (Mg^{2+}, SO_4^{2-} and Ca^{2+}) was about less than half a day (See Fig. 5.9). Another interesting point to observe is the amount of ions (Mg^{2+} and SO_4^{2-}) lost in the core for both intact and fractured chalks. We can clearly see that higher amount of magnesium and sulfate was lost in the intact core than the fractured core. Therefore, the high amount of loss of magnesium and sulfate inside the intact core triggered larger chemical deformation compared to the fractured chalk.

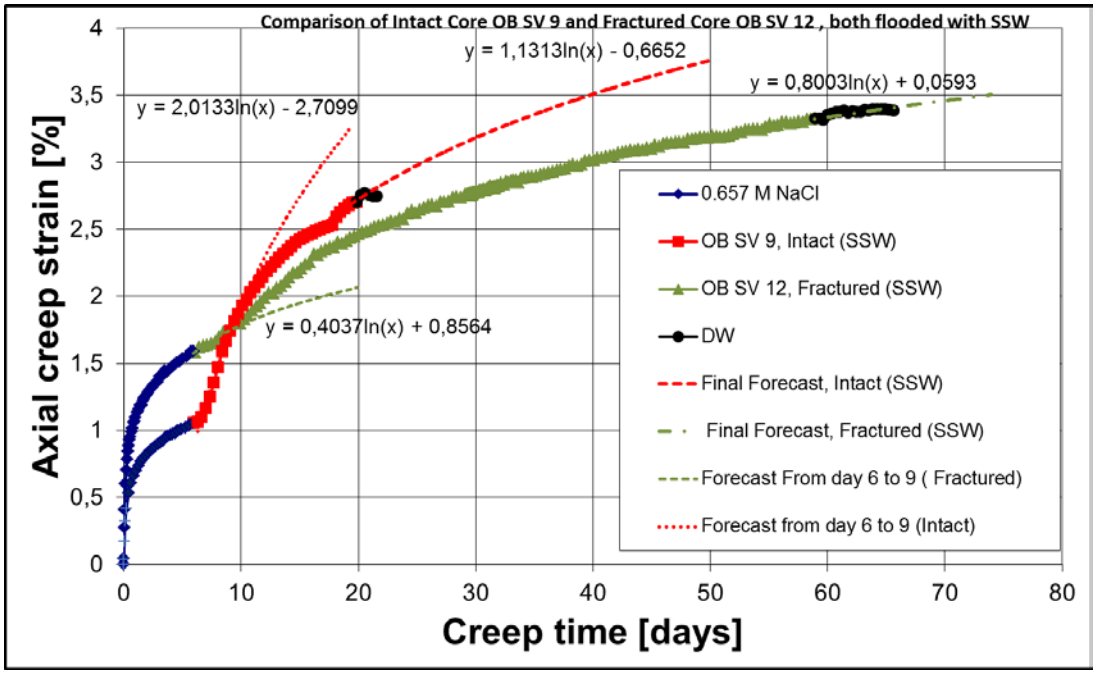

Figure 5.10: Axial creep strain [%] is plotted as a function of Creep time [days] for both intact (OB SV 9) and fractured (OB SV 12) cores during SSW flooding. The intact chalk sample showed higher creep strain rate (9.28%/decade) than the fractured chalk sample (6.56%/decade).This could be because of the difference transport mechanisms of fluids in fractured and intact cores. As a result, high amount of sulfate and magnesium was lost in the intact core than the fractured core

The effects of fractures further examined by performing another two mechanical tests on two Mons cores (one fractured and one intact) but the flooding fluid used for this case was 0.219 M $MgCl_2$. Fig 5.11 shows the comparison of two Mons Chalk samples that were flooded with $MgCl_2$.We can clearly see that the intact core (OB SV 6) had deformed more with final creep strain rate of 6%/decade compared to the fractured chalk which was deformed with 5.98%/decade. The creep strain rates are more or less similar for both fractured (OB SV 4) and intact (OB SV 6) cores flooded with 0.219M $MgCl_2$. This suggests that the effect of fractures in reducing creep strain is more magnified when the flooding fluid is SSW. This might be because of the presence of sulfate, which can cause extra deformation, in SSW. Needless to mention, the chemical analyses results showed that the breakthrough time for the divalent ions in the intact core (OB SV 6) was longer than the fractured core (OB SV 4). Moreover, the amount of ions (Mg^{2+} and SO_4^{2-}) lost in the intact core was higher than the fractured core (see figs. 5.6 and 5.7).

Therefore, based on our observation, the presence of fractures in cores would actually allay chemical deformation as the travel path of the chemical ions injected eased by the fractures inside the core. This minimizes the probability of chalk surface- fluid interaction; as a result less water weakening effect. However, this does not mean that the presence of fractures inside the cores will totally stop the water weakening effects; rather the water weakening effect would be mostly restricted to the fracture walls at first; but then the injected fluid would diffuse from the fracture walls into the core matrix to cause extra deformation. We also confirmed that the formation of magnesium bearing minerals on the fractured.

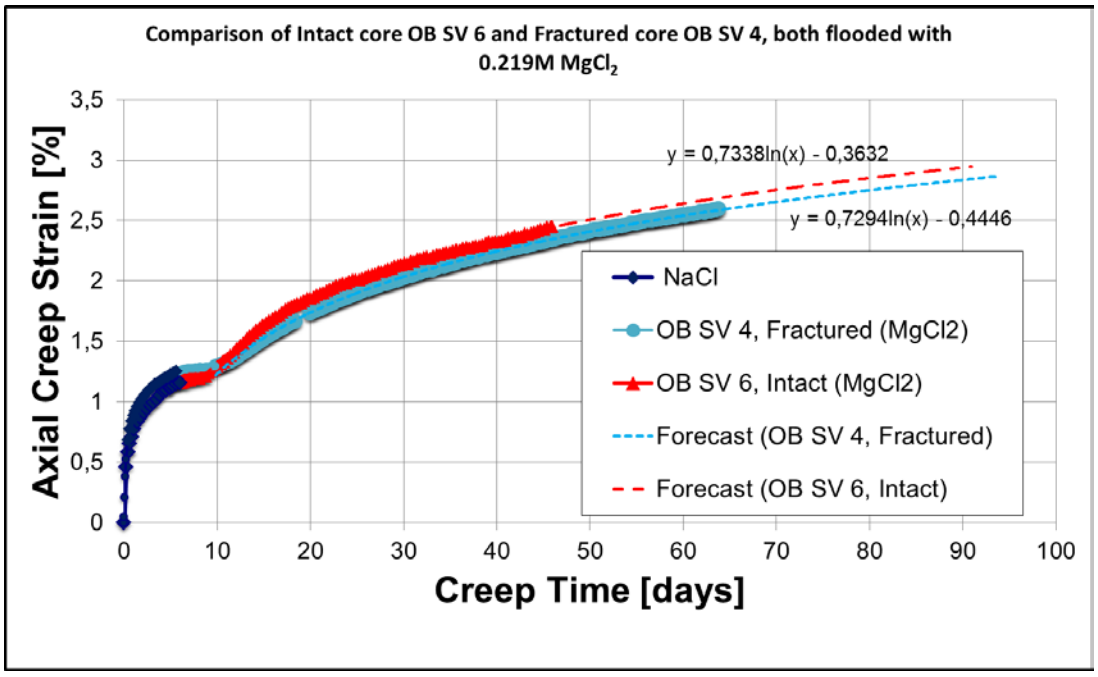

Figure 5.11: Axial creep strain [%] is plotted as a function of Creep time [days] for both intact (OB SV 6) and fractured (OB SV 4) cores during 0.219 M $MgCl_2$ flooding. The intact chalk sample showed higher creep strain rate than the fractured chalk sample although the creep strain rates for both of the cores are very comparable. This similarity between the creep strains of the two cores flooded with 0.219M $MgCl_2$ only explained by the absence of sulfate, which causes extra deformation, in the 0.219M $MgCl_2$.

5.2.5 Evidence of mineral precipitation on the fracture walls

Chemically induced weakening seems to be triggered by precipitation of secondary minerals which further cause increased dissolution. From previous experiment these precipitates could easily be found dominantly in the fracture. Actually these precipitates seem to contribute to healing of these fractures (like kind of gluing the

fracture together). Madland et al. (2011) verified the precipitation of new minerals in the chalk matrix of cores flooded with $MgCl_2$ and SSW with low NaCl concentration using scanning electron microscopy with X-ray microanalysis (SEM-EDS). The same procedure was used in this study as well to verify the presence of newly formed magnesium bearing minerals on the fracture walls. Fractured core OB SV 12 flooded with SSW was studied using SEM-EDS. The analysis showed very high magnesium content (1.94-2.09wt %) at the walls of the fracture compared to inside the core matrix (0.39-0.56wt %) (See Fig. 5.12). This clearly verified the notion that most of the magnesium injected was lost on the walls of the fractures and that the fluid interaction with core matrix is minimal as compared to intact cores. Also, this confirms the hypothesis that the travel path of the chemical ions injected was mainly through the fractures although some of the fluids injected would diffuse into the core matrix.

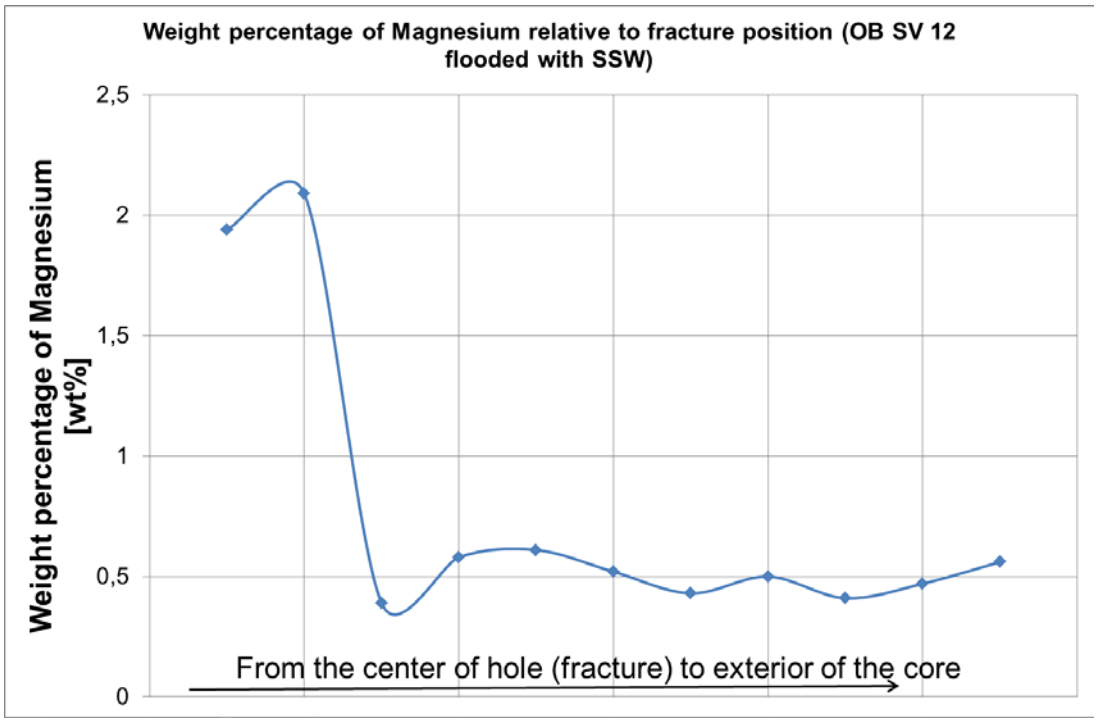

Figure 5.12: Weight percentage of magnesium [wt%] relative to fracture position for fractured core OB SV 12 flooded with SSW. High weight percentage of magnesium was observed on the fracture walls as compared to inside the core matrix (far from the fracture wall).

We further investigated the formation of magnesium bearing minerals using SEM analysis. The analysis showed that the fracture walls seemed altered; may be

because of the formation of magnesium bearing minerals (see Fig 5.13). The core matrix far from the fracture walls, however, seemed relatively clean and the coccolith rings looked undamaged (see Fig 5.14). According to Madland et al. (2011), there are at least two different types of newly precipitated magnesium-bearing minerals: silicate mineral with a clay-like appearance and magnesium-bearing carbonate minerals. However; the formation of anhydrite ($CaSO_4$) is very unlikely since the chemical analysis of fractured core OB SV 12 showed insignificant amount of loss of sulfate to form $CaSO_4$.

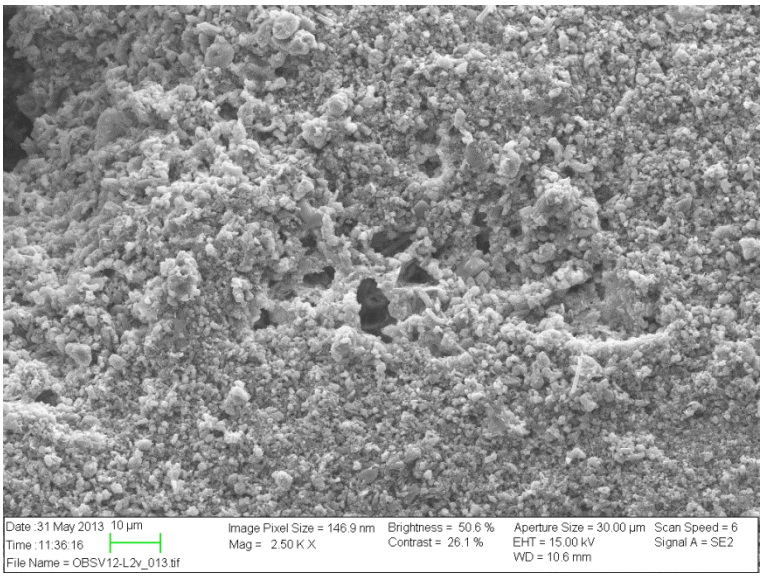

Figure 5.13: SEM micrograph of fractured chalk core OB SV 12 after flooding with SSW at the fracture walls. The fracture walls looked damaged and it seemed the coccolith rings are covered with (clays?).

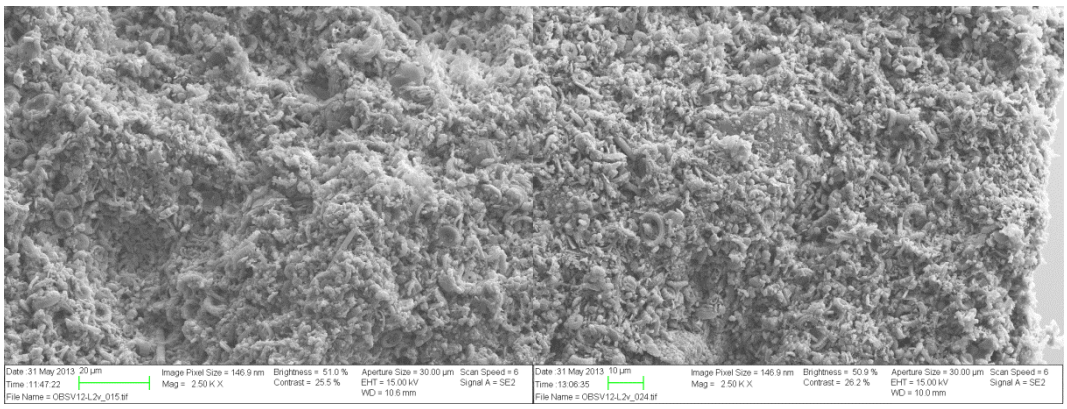

Figure 5.14: SEM micrograph of fractured chalk core OB SV 12 after flooding with SSW inside the core matrix (far from fracture walls). The matrix looks relatively clean and one might see the coccolith rings undamaged and not covered by clay-like minerals or magnesium-bearing minerals.

6 CONCLUSIONS

The effects of flooding brines and presence of fractures inside cores on the mechanical properties of five Mons chalk samples have been carefully studied using hydraulically operated triaxial cells at 130^{o}C. Based on the results observed, the following conclusions have been drawn.

- Regardless of the fractures introduced and the small porosity variations, all the tested Mons chalk samples had shown very similar yield and K-values during hydrostatic loading.
- Comparisons during creep phase (Impact of Flooding brine).
  - ✓ The intact core flooded with SSW had shown superior creep strain rate (9.28%/decade) than intact core flooded with 0.219M $MgCl_2$ (6%).
  - ✓ The fractured chalk flooded with SSW had been deformed with higher creep strain rate of 6.56%/decade compared to the fractured cores flooded with 0.657M NaCl (1.75%/decade) and 0.219M $MgCl_2$ (5.98%/decade).
  - ✓ Therefore, the impact of flooding brine is magnified in intact cores than fractured cores.
  - ✓ Both fractured and intact chalks showed flattening of creep curve when flooded with 0.219M $MgCl_2$ for a period of 3-4 days.
- Comparisons during creep phase (Impact of Fractures)
  - ✓ The intact chalk had shown higher creep strain rate (9.28%/decade) than the fractured core chalk sample (6.56%7decade) during SSW flooding
  - ✓ The intact chalk had shown higher creep strain rate (6%/decade) than the fractured core chalk sample (5.98%7decade) during 0.219M $MgCl_2$ flooding.
  - ✓ Therefore, the impact of fractures is magnified in reducing the chemical deformation during SSW flooding, because of SO_4^{2-}.
- Based on the comparisons, the presence of fractures inside the fractured cores resulted in lower amount of deformation compared to intact cores. However, the presence of fractures had not hindered the water weakening effect.

- Fluid transport Mechanism
  - ✓ In intact cores, the flooding fluid flow through the entire core matrix as evidenced by the chemical analysis. As a result, the degree of the amount of Mg^{2+} and SO_4^{-2} ions lost in the core and the production of Ca^{2+} is higher in intact cores.
  - ✓ In Fractured cores, the flooding fluid not only flow through the fractures, but also diffuses into the core matrix. This is evidenced by high amount of loss of Mg^{2+} and gain of Ca^{2+}. This corresponds to the fracture/matrix flow model developed by Anderson & Evje (2012)
- Governing mechanism for water weakening effects for both fractured and intact chalks seemed to be not only substitution process but also mainly precipitation of minerals which results dissolution of calcium carbonate as it was confirmed previously by Madland et al. (2011). The formation of new minerals was confirmed by SEM-EDS analysis, which showed the presence of magnesium-bearing minerals in/nearby the fracture. Further, the variations seen between the mechanical porosities and mechanical plus chemical porosities clearly indicate the formation of new minerals.

- Recommendation for future work

  - ✓ Experiments to be carried out with different chalk type, flooding brine flow rate and fracture geometry. Since creep experiments are time dependent, experiments should be run for a longer periods than what has been done in this work.

7 REFERENCES

Ahmed, T. (2001). Reservoir Engineering Handbook (2nd Edition): Elsevier.

Andersen, P., & Evje, S. (2012). *Two-phase flow in a fissurized-porous media.* Paper presented at the AIP Conference Proceedings.

Austad, T., Strand, S., Madland, M. V., Puntervold, T., & Korsnes, R. I. (2008). Seawater in Chalk: An EOR and Compaction Fluid. *SPE Reservoir Evaluation & Engineering, 11*(4), pp. 648-654. doi: 10.2118/118431-pa

Craze, R. C. (1950). *Performance of Limestone Reservoirs*.

Delage, P., Cui, Y. J., & Schroeder, C. (1996). *Subsidence And Capillary Effects In Chalks*. http://www.onepetro.org/mslib/app/Preview.do?paperNumber=ISRM-EUROCK-1996-160&societyCode=ISRM

Fjær, E., Holt, R. M., Horsrud, P., Raaen, A. M., & Risnes, R. (2008). Petroleum Related Rock Mechanics (2nd Edition) (2nd ed.): Elsevier.

Geitle, K. (2013). *Chemical induced compaction in fractured and intact chalks.* (Master's Master's), University of Stavanger, Stavanger.

Gutierrez, M., Oino, L. E., & Hoeg, K. (2000). The Effect of Fluid Content on the Mechanical Behavior of Fractures in Chalk. *Rock Mechanics and Rock Engineering*.

Haddadi, D. (2013). *An investigation of permeability and porosity evolution of Kansas chalk under in-situ conditions.* (Master's Master's Thesis), University of Stavanger Stavanger.

Hallenbeck, L. D., Sylte, J. E., Ebbs, D. J., & Thomas, L. K. (1991). Implementation of the Ekofisk Field Waterflood. *SPE Formation Evaluation, 6*(3), 284-290. doi: 10.2118/19838-pa

Hedegaard, K., & Graue, A. (2011). *Does Wettability Affect the Strength of Chalk?* http://www.onepetro.org/mslib/app/Preview.do?paperNumber=ARMA-11-599&societyCode=ARMA

Korsnes. (2007). *Chemical induced water weakening of chalk by fluid-rock interactions - A mechanistic study*. (PHILOSOPHIAE DOCTOR), University of Stavanger, 2007.

Korsnes, R., Madland, M., & Austad, T. (2006). Impact of brine composition on the mechanical strength of chalk at high Temperature *Eurock 2006: Multiphysics Coupling and Long Term Behaviour in Rock Mechanics* (pp. 133-140): Taylor & Francis.

Korsnes, R., Strand, S., Hoff, Pedersen, T., Madland, M., & Austad, T. (2006). Does the chemical interaction between seawater and chalk affect the mechanical properties of chalk? *Eurock 2006: Multiphysics Coupling and Long Term Behaviour in Rock Mechanics* (pp. 427-434): Taylor & Francis.

Korsnes, R. I., Wersland, E., Austad, T., & Madland, M. V. (2008). Anisotropy in chalk studied by rock mechanics. *Journal of Petroleum Science and Engineering, 62*(1–2), 28-35. doi: http://dx.doi.org/10.1016/j.petrol.2008.06.004

Lykke, M. M. (2005). *Displacement of Oil by Water Flooding in Fractured Chalk.* (PhD), Technical University of Denmark.

Madland, M., Midtgarden, K., Manafov, R., Korsnes, R., Kristiansen, T., & Hiorth, A. (2008). *The effect of temperature and brine composition on the mechanical strength of kansas chalk.* Paper presented at the International Symposium SCA.

Madland, M. V., Hiorth, A., Omdal, E., Megawati, M., Hildebrand-Habel, T., Korsnes, R. I., . . . Cathles, L. M. (2011). Chemical Alterations Induced by Rock–Fluid Interactions When Injecting Brines in High Porosity Chalks. *Transport in Porous Media, 87*(3), 679-702. doi: 10.1007/s11242-010-9708-3

Megawati, M., Hiorth, A., & Madland, M. V. (2012). The Impact of Surface Charge on the Mechanical Behavior of High-Porosity Chalk. *Rock Mechanics and Rock Engineering*, 1-18. doi: 10.1007/s00603-012-0317-z

Moore, C. H. (2001). *Carbonate Reservoirs: Porosity Evolution and Diagenesis in a Sequence Stratigraphic Framework*: Elsevier Science & Technology Books.

Omdal, E. (2010). *The Mechanical Behavior of Chalk Under Laboratory Conditions Simulating Reservoir Operations.* (PHILOSOPHIAE DOCTOR), University of Stavanger, Stavanger.

Powell, B. N., & Lovell, G. L. (1994). *Mechanisms of chalk compaction*. Paper presented at the Rock Mechanics in Petroleum Engineering, Delft, Netherlands. http://www.onepetro.org/mslib/app/Preview.do?paperNumber=00028132&societyCode=SPE

Puntervold, T., & Austad, T. (2007). *Injection of seawater and mixtures with produced water into North Sea chalk formation: Impact on wettability, scale formation and rock mechanics caused by fluid-rock interaction*. Paper presented at the SPE/EAGE Reservoir Characterization and Simulation Conference, Abu Dhabi, UAE. http://www.onepetro.org/mslib/app/Preview.do?paperNumber=SPE-111237-MS&societyCode=SPE

Risnes, R. (2001). Deformation and yield in high porosity outcrop chalk. *Physics and Chemistry of the Earth, Part A: Solid Earth and Geodesy, 26*(1–2), 53-57. doi: http://dx.doi.org/10.1016/S1464-1895(01)00022-9

Risnes, R., & Flaageng, O. (1999). Mechanical Properties of Chalk with emphasis on Chalk-Fluid Interactions and Micromechanical Aspects. *Oil & Gas Science and Technology - Rev. IFP, 54*(6), 751-758.

Risnes, R., Haghighi, H., Korsnes, R. I., & Natvik, O. (2003). Chalk–fluid interactions with glycol and brines. *Tectonophysics, 370*(1–4), 213-226. doi: http://dx.doi.org/10.1016/S0040-1951(03)00187-2

Roehl, P. O., & Choquette, P. W. (1985). *Carbonate petroleum reservoirs*. New York: Springer.

Schlumberger. Carbonate Resrvoirs. Retrieved February 10, 2013, from http://www.slb.com/services/technical_challenges/carbonates.aspx?entry=ad_google_cr_carbonate&gclid=CKjJmJrP6LcCFQeW3godglQAHw

Sheng, J. J. (2011). Modern Chemical Enhanced Oil Recovery - Theory and Practice: Elsevier.

Sylte, J. E., Thomas, L. K., Rhett, D. W., Bruning, D. D., & Nagel, N. B. (1999). *Water Induced Compaction in the Ekofisk Field*. Paper presented at the SPE Annual Technical Conference and Exhibition, Houston, Texas. http://www.onepetro.org/mslib/app/Preview.do?paperNumber=00056426&societyCode=SPE